Article

Immunity

Interleukin-33-activated neuropeptide CGRP-producing memory Th2 cells cooperate with somatosensory neurons to induce conjunctival itch

Graphical abstract

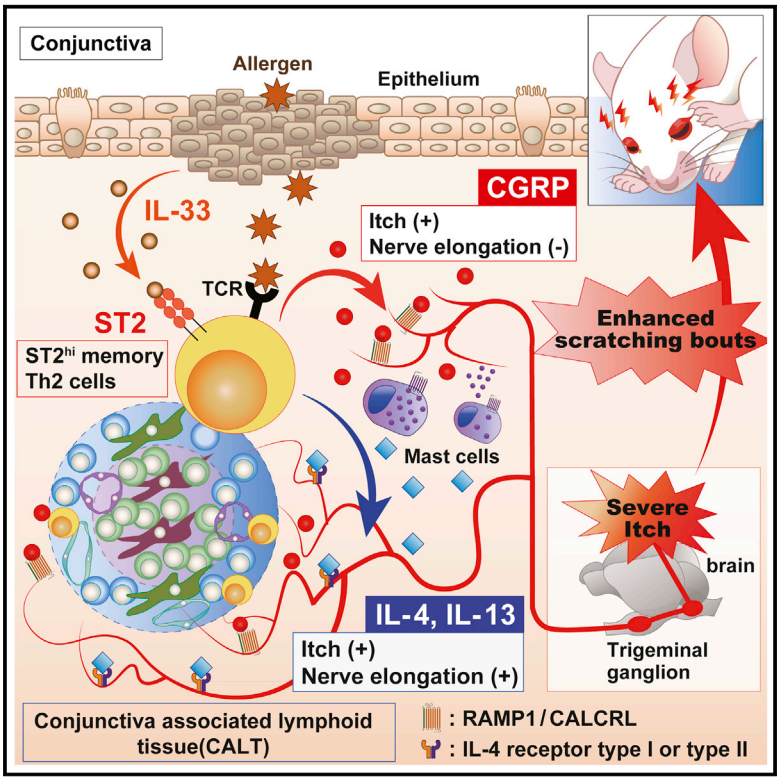

Highlights

- The IL-33-ST2 axis induces axonal elongation in allergic conjunctivitis
- A population of memory pathogenic Th2 cells in the conjunctiva express *Il1rl1* and *Calca*
- CGRP produced by memory pathogenic Th2 cells drives severe itch in conjunctivitis
- CALT structure formation with axonal elongation is observed in human giant papillae

Authors

Mikiko Okano, Kiyoshi Hirahara, Masahiro Kiuchi, ..., Akira Murakami, Nobuyuki Ebihara, Toshinori Nakayama

Correspondence

hiraharak@chiba-u.jp (K.H.), tnakayama@faculty.chiba-u.jp (T.N.)

In brief

Severe itch is a critical clinical symptom that interferes with the quality of life of patients with allergic conjunctival inflammation. Okano et al. demonstrate that the IL-33-ST2-CGRP-Ramp1 axis directs severe allergic inflammation-induced itch in chronic conjunctivitis via immune-neuronal interaction between memory pathogenic Th2 cells and peripheral pruriceptive neurons in both mice and humans.

Okano et al., 2022, Immunity *55*, 2352–2368
December 13, 2022
https://doi.org/10.1016/j.immuni.2022.09.016

CellPress

CellPress

Immunity

Article

Interleukin-33-activated neuropeptide CGRP-producing memory Th2 cells cooperate with somatosensory neurons to induce conjunctival itch

Mikiko Okano,[1,2,7] Kiyoshi Hirahara,[1,3,7,*] Masahiro Kiuchi,[1,7] Miki Onoue,[1,4,7] Chiaki Iwamura,[1] Kota Kokubo,[1] Takahisa Hishiya,[1] Yuki Morimoto,[1] Yuzuru Ikehara,[5] Akira Murakami,[4] Nobuyuki Ebihara,[2] and Toshinori Nakayama[1,6,8,*]

[1]Department of Immunology, Graduate School of Medicine, Chiba University, 1-8-1 Inohana, Chuo-ku, Chiba 260-8670, Japan
[2]Department of Ophthalmology, Juntendo University Urayasu Hospital, Chiba 279-0021, Japan
[3]AMED-PRIME, AMED, 1-8-1 Inohana, Chuo-ku, Chiba 260-8670, Japan
[4]Department of Ophthalmology, Juntendo University School of Medicine, Tokyo 113-8431, Japan
[5]Department of Molecular and Tumor Pathology, Graduate School of Medicine, Chiba University, 1-8-1 Inohana, Chuo-ku, Chiba 260-8670, Japan
[6]AMED-CREST, AMED, 1-8-1 Inohana, Chuo-ku, Chiba 260-8670, Japan
[7]These authors contributed equally
[8]Lead contact
*Correspondence: hiraharak@chiba-u.jp (K.H.), tnakayama@faculty.chiba-u.jp (T.N.)
https://doi.org/10.1016/j.immuni.2022.09.016

SUMMARY

Allergic conjunctivitis is a chronic inflammatory disease that is characterized by severe itch in the conjunctiva, but how neuro-immune interactions shape the pathogenesis of severe itch remains unclear. We identified a subset of memory-type pathogenic Th2 cells that preferentially expressed *Il1rl1*-encoding ST2 and *Calca*-encoding calcitonin-gene-related peptide (CGRP) in the inflammatory conjunctiva using a single-cell analysis. The IL-33-ST2 axis in memory Th2 cells controlled the axonal elongation of the peripheral sensory C-fiber and the induction of severe itch. Pharmacological blockade and genetic deletion of CGRP signaling *in vivo* attenuated scratching behavior. The analysis of giant papillae from patients with severe allergic conjunctivitis revealed ectopic lymphoid structure formation with the accumulation of IL-33-producing epithelial cells and CGRP-producing pathogenic $CD4^+$ T cells accompanied by peripheral nerve elongation. Thus, the IL-33-ST2-CGRP axis directs severe itch with neuro-reconstruction in the inflammatory conjunctiva and is a potential therapeutic target for severe itch in allergic conjunctivitis.

INTRODUCTION

Allergic conjunctivitis accompanies chronic inflammation of the conjunctiva due to exposure to airborne allergens, such as pollen and house dust mites (Azari and Barney, 2013). Patients with allergic conjunctivitis often suffer from other allergic diseases (Azari and Barney, 2013). Allergic conjunctivitis is one of the most common allergic diseases worldwide and affects up to 40% of the population in the USA (Azari, and Barney, 2013). Allergic conjunctivitis is characterized by redness, swelling, tearing, and severe itch in the conjunctiva. The hallmark of allergic conjunctivitis is severe itch, which impairs the quality of life, particularly in patients with moderate-to-severe symptoms (Azari and Barney, 2013; Leibowitz, 2000; Sy and Bielory, 2013). Severe itch in the conjunctiva often causes visual complications because of chronic eye rubbing (Huang et al., 2018). Topical steroids, which are most commonly used to treat intractable allergic conjunctivitis with severe itch, can also cause cataract and glaucoma (Azari and Barney, 2013; Ram and Agarwal, 2014).

Somatosensory neurons located in the trigeminal ganglion (TG) regulate itch in the conjunctiva during allergic conjunctivitis (Huang et al., 2018; Usoskin et al., 2015). Type 2 cytokines, such as interleukin (IL)-4 and IL-13, which are produced by immune cells, directly activate sensory neurons to induce itch during allergic inflammation in the skin (Oetjen et al., 2017). Other type 2 cytokines, such as thymic stromal lymphopoietin (TSLP), IL-31, and IL-33 are also involved in shaping the pathogenesis of itch in allergic dermatitis (Liu et al., 2016; Wilson et al., 2013; Yamamura et al., 2017). However, the precise cellular and molecular mechanisms that regulate severe itch in the conjunctiva during allergic conjunctivitis have been uncertain.

Memory T cells protect hosts against previously encountered pathogens (Manz et al., 2005; Sallusto et al., 2004), but they also play critical roles in the pathogenesis of chronic inflammatory diseases (Nakayama et al., 2017; Ruterbusch et al., 2020). In particular, memory-type pathogenic T helper 2 (Th2) cells are involved in shaping the pathogenesis of chronic allergic inflammatory diseases (Endo et al., 2015; Morimoto et al., 2018). IL-5-producing memory-type pathogenic Th2 cells recruit and

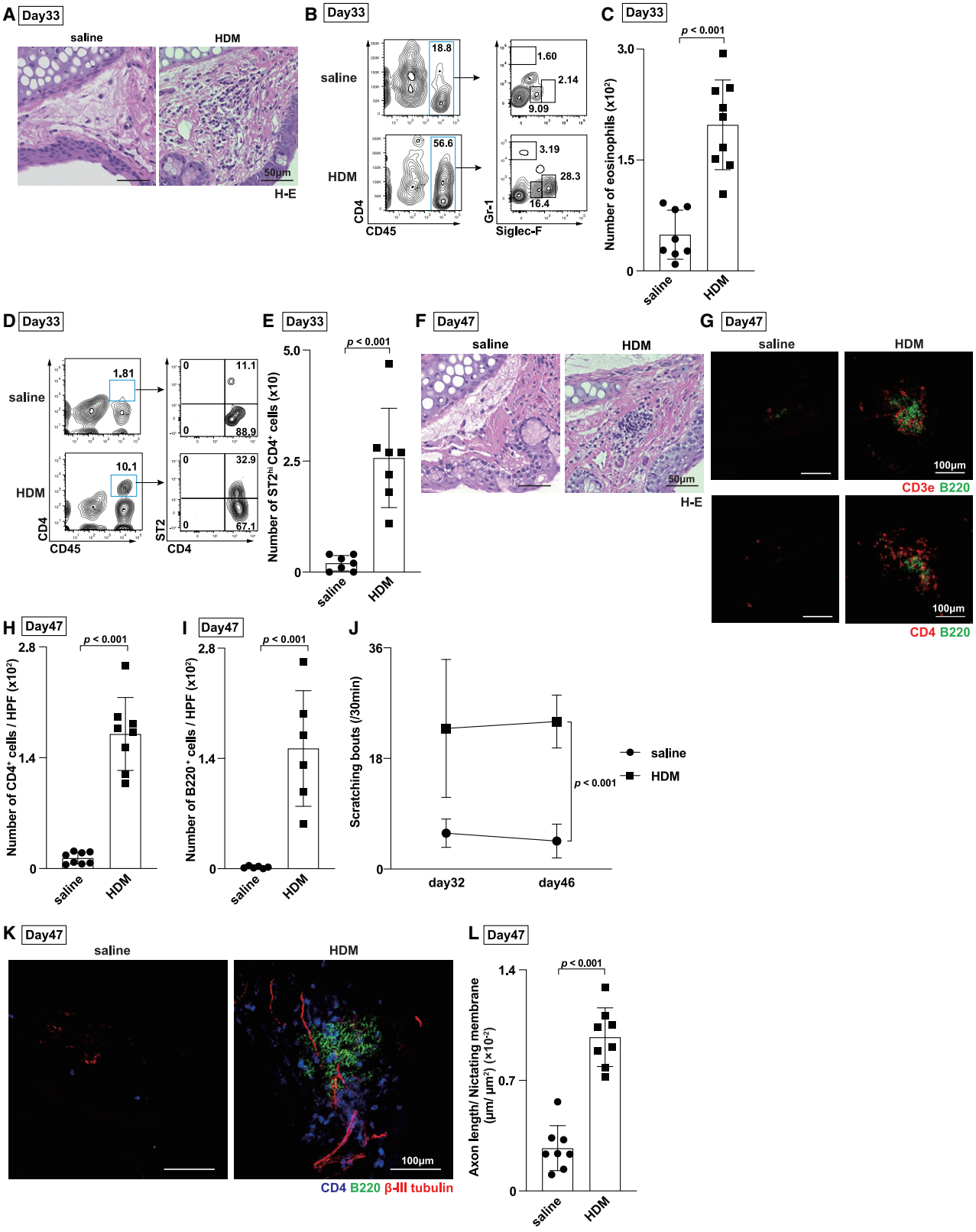

Figure 1. Repeated exposure to house dust mite (HDM) via eye drops caused allergic inflammation and itch

(A–L) BALB/c mice were immunized with HDM and 2-hydroxypropyl-beta-cyclodextrin (HP-β-CD), followed by repeated exposure to HDM via eye drops for 3 weeks, as indicated in Figure S1A.

(legend continued on next page)

activate eosinophils and amphiregulin-producing memory-type pathogenic Th2 cells induce fibrotic responses, which indicates the functional diversity of memory-type pathogenic Th2 cells (Endo et al., 2015; Morimoto et al., 2018). IL-5-producing pathogenic Th2 cells have been also detected in the peripheral blood of patients with eosinophilic gastrointestinal diseases and allergic diseases (Mitson-Salazar et al., 2016; Seumois et al., 2016; Wambre et al., 2017). In conjunctival allergic inflammation, patients with severe allergic conjunctivitis, such as atopic keratoconjunctivitis (AKC) and vernal keratoconjunctivitis (VKC) show the massive infiltration of effector Th2 cells and memory-type CD45RO^{+}CD4^{+} T cells in the conjunctiva (Leonardi, 2002). The histological analysis of giant papillae from the patients with AKC or VKC reveals the formation of the lymphoid clusters containing a marginal T cell zone and separate B cell clusters accompanied by follicular dendritic cells (FDCs), resident dendritic cells (DCs), high endothelial venules (HEVs), and lymphatics, which are called conjunctiva-associated lymphoid tissue (CALT) (Matsuda et al., 2010). However, the pathogenic role of memory Th2 cells in shaping severe itch in allergic conjunctivitis remains unknown.

We investigated the cellular and molecular mechanisms that control the pathogenesis of severe itch in allergic conjunctivitis. We found that repeated exposure to house dust mite (HDM) via eye drops resulted in increased bouts of scratching and axonal elongation of sensory neurons, accompanied by the enhanced infiltration of ST2^{hi} CD4^{+} T cells and the induction of the CALT structure in HDM-immunized mice. Scratching bouts and the axonal elongation in the conjunctiva occurred in a T-cell-dependent manner via the IL-33-ST2 axis. Single-cell RNA sequencing (scRNA-seq) revealed the heterogeneity of ST2^{hi} memory-type pathogenic Th2 cells, including calcitonin-related polypeptide alpha (*Calca*)-expressed ST2^{hi} memory-type Th2 cells in the HDM-induced allergic conjunctiva. IL-33 induced the expression of *Calca* in ST2^{hi} memory-type pathogenic Th2 cells. The IL-33-ST2 axis regulated the severity of itch and the axonal elongation in the conjunctiva in the model of allergic conjunctivitis. Pharmacological blockade and genetic deletion of calcitonin-gene-related peptide (CGRP) signaling, which is encoded by *Calca*, resulted in the attenuation of severe itch *in vivo*. The analysis of the giant papillae of patients with severe allergic conjunctivitis revealed the increased infiltration of memory-type CD45RO^{hi}CD4^{+} T cells accompanied by the accumulation of IL-33-producing epithelial cells and the peripheral nerve elongation. Thus, the IL-33-ST2-CGRP axis directs allergic inflammation-induced severe itch, and these molecules may be potential therapeutic targets for intractable chronic itch during chronic allergic inflammation.

RESULTS

Repeated exposure to HDM via eye drops induces itch accompanied by axonal elongation

Severe itch is a critical clinical symptom that interferes with the quality of life of patients with allergic conjunctival inflammation (Azari and Barney, 2013). To investigate the neuro-immunological events that occur during allergic conjunctival inflammation, we developed an experimental model in which mice were immunized with house dust mite (HDM) antigen and 2-hydroxypropyl-beta-cyclodextrin (HP-β-CD) as an adjuvant, followed by repeated exposure to HDM antigen via eye drops for 3 weeks (Onishi et al., 2015) (Figure S1A). These HDM-treated mice showed conjunctival hyperemia together with the enhanced infiltration of SiglecF^{+}Gr-1^{-} eosinophils into the palpebral conjunctiva (Figures S1B, S1C, and 1A–1C). HDM exposure resulted in increased numbers of infiltrating CD4^{+} T cells, which expressed the IL-33 receptor, ST2 (Figures 1D and 1E). A lymphoid cluster consisting of CD3^{+} cells and B220^{+} cells was formed in the nictitating membrane on day 47 (Figures 1F–1I). Importantly, prolonged and enhanced scratching bouts were observed in mice treated with HDM (Figure 1J). A histological analysis revealed the axonal elongation of the peripheral nerves around the lymphoid clusters of mice that underwent HDM exposure (Figures 1K and 1L). Altogether, HDM-induced conjunctival inflammation caused severe itch, together with the elongation of the peripheral nerves in the conjunctiva.

HDM-induced severe itch accompanied by axonal elongation is T cell dependent

To characterize the immune cells in the HDM-induced allergic conjunctiva, we generated scRNA-seq profiles with 5,258 CD45^{+} immune cells collected from conjunctivae from control and HDM-treated mice (Figure S2A). Overall, we identified 23

(A) Representative images of hematoxylin and eosin (H&E) staining in the conjunctiva of mice treated with saline (saline) or HDM (HDM) on day 33. Scale bars, 50 μm. n = 4 mice per group from 2 independent experiments.
(B and C) Representative cell surface staining profiles of Siglec-F and Gr-1 in CD45^{+} cells from the conjunctiva (B) and pooled data showing the proportion of Siglec-F^{+}Gr-1^{-} eosinophils in the total population from the conjunctiva (C). n = 8 mice (saline) and n = 9 mice (HDM) from 2 independent experiments.
(D and E) Representative cell surface staining profiles of CD4 and ST2 in CD45^{+} cells from the conjunctiva on day 33 (D) and pooled data showing the absolute number of ST2^{hi} CD4^{+} T cells (E). n = 7 mice per group from 2 independent experiments.
(F) Representative images of H&E staining in the conjunctiva of the indicated mice. Scale bars, 50 μm. n = 4 mice from 2 independent experiments.
(G) A representative confocal micrograph of the conjunctiva stained with anti-CD3ε (red), anti-CD4 (red) and anti-B220 (green) of the indicated mice. Scale bars, 100 μm. n = 3 mice from 2 independent experiments.
(H) Absolute number of CD4^{+} cells in the conjunctiva. n = 8 mice per group from 2 independent experiments.
(I) Absolute number of B220^{+} cells in the conjunctiva. n = 6 mice per group from 2 independent experiments.
(J) Absolute number of scratching bouts. n = 6 mice (saline) and n = 8 mice (HDM) from 2 independent experiments.
(K) A representative confocal micrograph of the conjunctiva stained with anti-CD4 (blue), anti-B220 (green), and anti-β-III tubulin (red) on day 47. Scale bars, 100 μm. n = 8 mice per group from 2 independent experiments.
(L) Axon length per area of nictitating membrane of the same sample analyzed in (K). Data are shown as the mean ± SD. p values were calculated by an unpaired t test (C, E, H, I, and L) or a two-way analysis of variance (ANOVA) (J).
See also Figure S1.

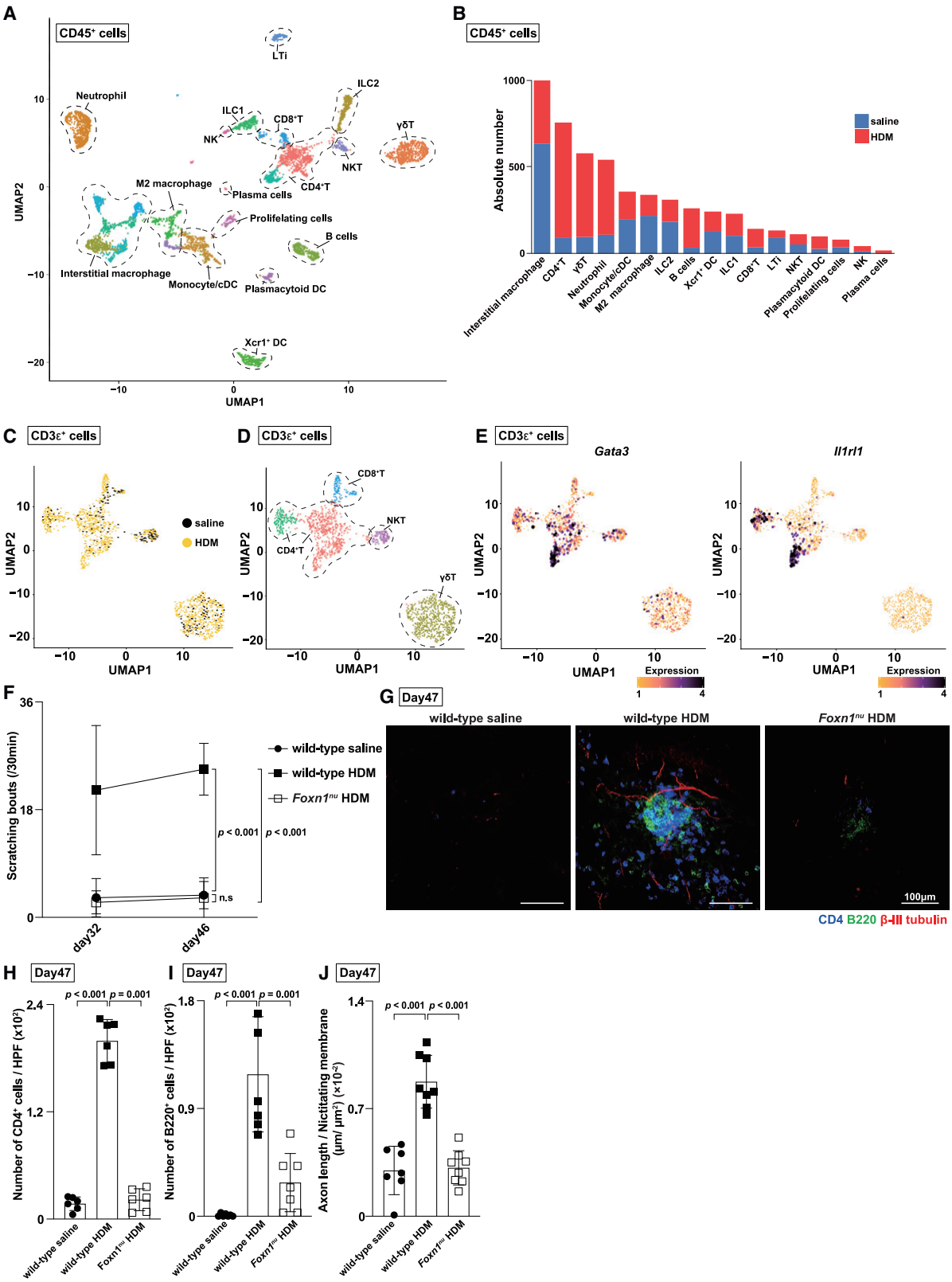

Figure 2. HDM-induced severe itch and axonal elongation were T cell dependent

(A–E) CD45⁺ cells were isolated by fluorescence-activated cell sorting (FACS) from the conjunctiva of mice treated with saline or HDM and analyzed by scRNA-seq. n = 13 mice (saline) and n = 11 mice (HDM) from 2 independent experiments.

(legend continued on next page)

clusters in an unbiased manner based on differentially expressed genes and inferred cluster identities based on the expression of marker genes (Figures 2A and S2B). HDM-treatment induced an increase in the number of CD45$^+$ cells in inflamed conjunctivae (Figure 2B red bars). The extensive infiltration of CD3ε^+ T cells (Figure 2C yellow dots), especially that of CD3ε^+CD4$^+$ T cells (Figures 2D and S2C), was revealed in the inflamed conjunctivae. Approximately one-third of infiltrating CD4$^+$ T cells expressed *GATA binding protein 3* (*Gata3*), which showed considerable transcriptional overlap with *Il1rl1* in Uniform Manifold Approximation and Projection (UMAP) (Figure 2E). *Foxn1*^{nu} mice, which are genetically T-cell-deficient due to the loss of global deficiency of Foxn1, showed the significant amelioration of scratching bouts in comparison with wild-type mice (Figure 2F). A lymphoid cluster consisting of CD4$^+$ cells and B220$^+$ cells was formed in the nictitating membrane in wild-type mice, but not in *Foxn1*^{nu} mice (Figures 2G–2I). Importantly, a histological analysis revealed the axonal elongation of the peripheral nerves in the conjunctiva in wild-type mice, but not *Foxn1*^{nu} mice (Figures 2G and 2J). In contrast, genetically eosinophil-lacking ΔdblGATA mice due to the mutation of Gata1 promoter region showed a similar increase in scratching bouts and axonal elongation to wild-type mice (Figures S2D–S2G). These results indicated that the HDM-induced conjunctival itch together with axonal elongation was T cell dependent.

Itch with axonal elongation in the conjunctiva was induced by repeated exposure to ovalbumin (OVA) in the presence of antigen-specific memory Th2 cells

We next sought to investigate the role of antigen-specific memory Th2 cells in shaping the pathogenesis of itch during conjunctival inflammation. To this end, we established another experimental allergic conjunctivitis model in which mice were adoptively transferred with ovalbumin (OVA)-specific memory Th2 cells, followed by repeated exposure to OVA and cholera toxin via eye drops (Figure S3A). Substantial conjunctival inflammation was detected immediately after the final exposure to OVA on day 23, irrespective of the adoptive transfer of OVA-specific memory Th2 cells (Figures S3B and S3C). In addition, the accumulation of inflammatory cells, including eosinophils in the conjunctiva was observed, irrespective of the adoptive transfer of OVA-specific memory Th2 cells (Figures S3D and S3E). However, mice with repeated exposure to OVA showed the formation of small conjunctiva-associated lymphoid tissue (CALT) structures in the conjunctiva on day 23 (Figure S3F). 2 weeks after the final administration of OVA (day 37), the accumulation of inflammatory cells—especially eosinophils—was still observed in the conjunctiva of mice with the adoptive transfer of memory Th2 cells (Figures 3A–3C). Moreover, the CALT structure developed with a separated T cell region and B cell region consisting of CD4$^+$ T cells, MHC class II$^+$ cells, B220$^+$ cells, CD11c$^+$ cells, and CD21-expressing follicular DCs accompanied by Lyve-1$^+$ lymphatics and CD31$^+$ small vessels in mice with the adoptive transfer of memory Th2 cells (Figures 3D–3F).

We next investigated the scratching behaviors of mice with adoptively transferred memory Th2 cells followed by repeated antigen exposure on days 22 and 36 (Figure 3G). On day 22, enhanced scratching bouts were observed in mice with repeated exposure to OVA with or without the adoptive transfer of memory Th2 cells (Figure 3G). Importantly, however, the enhanced scratching bouts were only detected in the mice with the adoptive transfer of memory Th2 cells on day 36 (Figure 3G). A histological analysis with immunofluorescence staining showed baseline elongation of the axons in all groups of mice on day 23 (Figures S3G and S3H). In contrast, on day 37, significantly enhanced elongation of the axons was only observed in mice with adoptively transferred memory Th2 cells (Figures 3H and 3I). These results indicate that antigen-specific memory Th2 cells were involved in shaping the pathogenesis of severe itch together with the formation of CALT structures and elongation of the peripheral nerves.

The IL-33-ST2 axis regulates the axonal elongation and severe itch in allergic conjunctival inflammation

Among epithelial cytokines, on day 23, *Il33* was upregulated in the conjunctiva from mice with adoptively transferred OVA-specific memory Th2 cells followed by repeated antigen exposure (Figure 4A). We focused on IL-33 because infiltrating CD4$^+$ T cells expressed the IL-33 receptor in the HDM-induced inflamed conjunctiva (see Figures 1D, 1E, and 2E right panel). To

(A) Twenty-three gene expression clusters (0–23) projected on a UMAP of the scRNA-seq libraries from the conjunctiva of mice treated with saline or HDM on day 33 as indicated in Figure S1A and colored according to the cellular subset.
(B) Absolute number of each cellular subset according to the treatment condition. Blue bars: cells of mice treated with saline. Red bars: cells of mice treated with HDM.
(C) A UMAP projection of CD3ε^+ cells selected from the original dataset highlighting the cellular source of mice treated with saline (black) and mice treated with HDM (yellow).
(D) A UMAP projection of CD3ε^+ cells selected from the original dataset, colored according to the cellular subset.
(E) The expression of *Gata3* (left) and *Il1rl1* (right) projected onto a UMAP.
(F–J) Wild-type mice and *Foxn1*^{nu} mice were treated with saline or HDM.
(F) Absolute number of scratching bouts on days 32 and 46 in wild-type mice treated with saline (wild-type saline) or HDM (wild-type HDM) and *Foxn1*^{nu} mice treated with HDM (*Foxn1*^{nu} HDM). n = 7 mice (wild-type saline), n = 8 mice (wild-type HDM) and n = 8 mice (*Foxn1*^{nu} HDM) from 2 independent experiments.
(G) A representative confocal micrograph of the conjunctiva stained with anti-CD4 (blue), anti-B220 (green), and anti-β-III tubulin (red). Scale bars, 100 μm. n = 7 mice (wild-type saline), n = 8 mice (wild-type HDM), and n = 8 mice (*Foxn1*^{nu} HDM) from 2 independent experiments.
(H) Absolute number of CD4$^+$ cells in the conjunctiva. n = 6 mice per group from 2 independent experiments.
(I) Absolute number of B220$^+$ cells in the conjunctiva. n = 6 mice (wild-type saline), n = 6 mice (wild-type HDM), and n = 7 mice (*Foxn1*^{nu} mice HDM) from 2 independent experiments.
(J) Axon length per area of nictitating membrane in the sample analyzed in (G). Data represent shown as the mean ± SD. p values were calculated by a one-way analysis of variance (ANOVA) (H–J) or two-way analysis of variance (F), ns, not significant.
See also Figure S2.

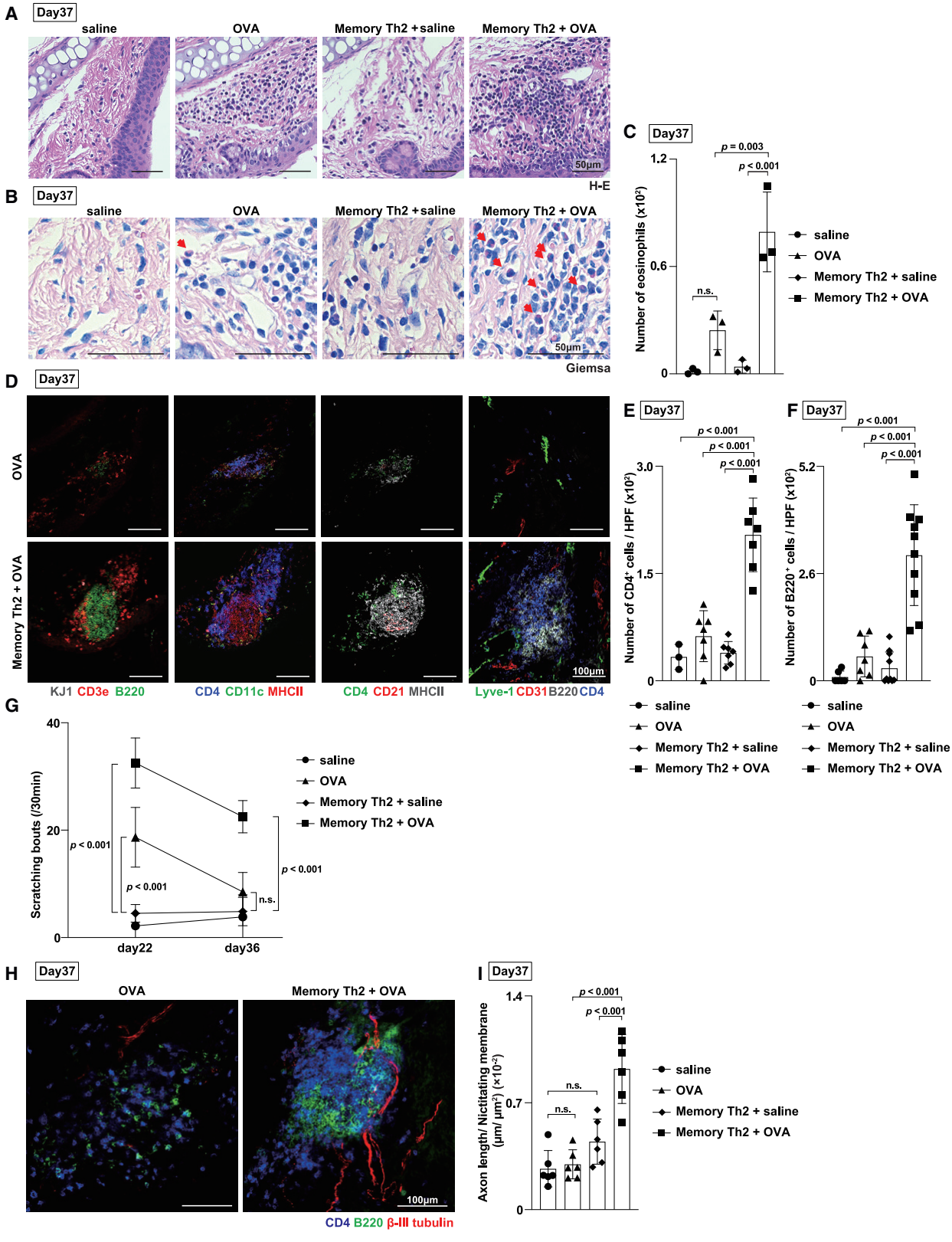

Figure 3. Antigen-specific memory Th2 cells induced the formation of CALT structures together with peripheral nerve elongation

(A–I) OVA-specific memory Th2 cells were transferred intravenously into BALB/c mice that were subsequently treated with saline or OVA, as indicated in Figure S3A.

(legend continued on next page)

determine the role of IL-33 in this allergic conjunctivitis model, OVA-specific memory Th2 cells were adoptively transferred to wild-type mice or *Il33*-deficient mice, followed by repeated exposure to OVA (Figure S4A). The size of the CALT structure was comparable between wild-type and *Il33*-deficient mice (Figures S4B and S4C). However, *Il33*-deficient mice showed ameliorated scratching bouts and decreased axonal elongation together with a decreased number of infiltrating eosinophils in comparison with wild-type mice (Figures 4B–4D, and S4D). Il1rl1$^{-/-}$ memory Th2 cells produced similar amounts of Th2 cytokines to wild-type Th2 cells (Figure S4E). However, mice that received Il1rl1$^{-/-}$ memory Th2 cells also showed ameliorated scratching bouts and a significant decrease in axonal elongation, accompanied by a decreased number of infiltrating eosinophils (Figures S4F–S4I). Mice that received Il1rl1$^{-/-}$ memory Th2 cells showed CALT structures with similar numbers of CD4$^+$ T cells and B cells in comparison with mice that received Il1rl1$^{+/+}$ memory Th2 cells (Figures S4G and S4H). Furthermore, HDM-induced severe itch and axonal elongation were significantly decreased in both *Il33*-deficient and *Il1rl1*-deficient mice (Figures S4J–S4N). These results indicate that the IL-33-ST2 axis regulated the severity of itch and peripheral nerve elongation in the conjunctiva in a model of allergic conjunctivitis.

ST2^{hi} memory Th2 cells expressed Calca and pharmacological blockade and genetic deletion of CGRP resulted in the amelioration of severe itch during allergic conjunctivitis

Next, we sought to identify the molecules expressed in ST2^{hi} memory Th2 cells that induce severe itch in our experimental model. To investigate the expression of itch-related genes in CD4$^+$ T cells *in vivo*, we analyzed our scRNA-seq datasets from the mice treated with HDM (Figures 2, 5A, and S5A). Among itch-related genes (Table S1), Cathepsin S (*Ctss*), a member of the peptidase C1 family, and Kallikrein-8 (*Klk8*), a serine protease, were upregulated in both subsets of memory Th2 cells and regulatory T (Treg) cells in the inflamed conjunctiva (Figure 5B). Calcitonin-related polypeptide alpha (*Calca*), a neuropeptide, was highly expressed in memory Th2 cells in the conjunctivae from the mice with repeated exposure to HDM (Figure 5B). At the single-cell level, the majority of *Calca* expressed cells appeared to be transcriptionally overlapped with *Il1rl1* expressed cells (Figures 5C and 5D). Indeed, the mRNA expression of *Calca* was significantly corelated with the expression of *Il1rl1* in infiltrating CD4$^+$ T cells (r = 0.24) (Figure 5E). We also re-assessed our previously established dataset that include global gene expression in ST2^{hi} antigen-specific memory Th2 cells following 3 days of *in vitro* IL-33 stimulation (Morimoto et al., 2018) (Figure S5B). We found that *Calca* was significantly upregulated in ST2^{hi} antigen-specific memory Th2 cells by IL-33 stimulation *in vitro* (Figure 5F). Quantitative RT-PCR confirmed that IL-33 stimulation induced the expression of *Calca* in ST2^{hi} memory Th2 cells (Figure 5G).

We next determined whether or not calcitonin-gene-related peptide (CGRP), which is encoded by the *Calca* gene, causes severe itch in the inflamed conjunctiva. Conjunctival administration of CGRP as well as administration of chloroquine resulted in enhanced scratching bouts in HDM-treated mice but not in control mice (Figures S5C and 5H). In contrast, the mice that were adoptively transferred with *Calca*-deficient memory Th2 cells showed significant amelioration of scratching bouts, with only slight effects on the axonal elongation (Figures 5I, 5J, and S5D–S5F). These results indicate that CGRP produced by ST2^{hi} memory Th2 cells causes severe itch during allergic conjunctival inflammation.

ST2^{hi} memory Th2 cells in the conjunctiva of the mice treated with HDM showed the enhanced expression of *Il4* and *Il13* (Figure 5B). Consistent with a previous report (Oetjen et al., 2017), the mice treated with anti-IL-4Rα antibody showed a significant decrease in scratching bouts compared with control mice (Figures S5G and 5K). Importantly, the mice treated with anti-IL-4Rα antibody also showed a significant decrease in axonal elongation compared with control mice (Figures S5H and 5L). These results indicate that Th2 cytokines, such as IL-4 and IL-13, are involved in the axonal elongation and severe itch in the inflamed conjunctiva in the HDM model.

Single-cell transcriptomes of inflamed trigeminal ganglion revealed pruriceptive neurons with specific expression of Calcrl and Ramp1

We next explored whether or not elongated nerves in the inflamed conjunctiva were derived from the trigeminal ganglion (TG). We performed experiments with retrograde labeling by injecting wheat germ agglutinin (WGA)-A488 dye into the

(A) Representative images of H&E staining in the conjunctiva from mice treated with saline (saline) or OVA (OVA) and memory Th2-cell-transferred mice treated with saline (memory Th2 + saline) or OVA (memory Th2 + OVA) on day 37. Scale bars, 50 μm. n = 6 mice per group from 2 independent experiments.
(B) Representative images of Giemsa staining in the conjunctiva of the indicated mice. Scale bars, 50 μm. n = 6 mice per group from 2 independent experiments.
(C) Absolute number of eosinophils in the conjunctiva of the indicated mice. n = 3 mice per group from 1 experiment.
(D) A representative confocal micrograph of the conjunctiva of the indicated mice stained with anti-KJ1 (gray), anti-CD3ε (red), and anti-B220 (green) (left column); anti-CD4 (blue), anti-CD11c (green), and anti-MHC class II (red) (left middle column); anti-CD4 (green), anti-CD21 (red), and anti-MHC class II (gray) (right middle column); anti-Lyve-1 (green), anti-CD31(red), anti-CD4 (blue), and anti-B220 (gray) (right column). Scale bars, 100 μm. n = 6 mice per group from 2 independent experiments.
(E) Absolute number of CD4$^+$ cells in the conjunctiva of the indicated mice. n = 3 mice (saline) and n = 7 mice (OVA), n = 7 mice (memory Th2 + saline), and n = 7 mice (memory Th2 + OVA) from 2 independent experiments.
(F) Absolute number of B220$^+$ cells in the conjunctiva of the indicated mice. n = 6 mice (saline), n = 7 mice (OVA), n = 10 mice (memory Th2 + saline), and n = 10 mice (memory Th2 + OVA) from 2 independent experiments.
(G) Absolute number of scratching bouts in the indicated mice. n = 6 mice per group from 2 independent experiments.
(H) A representative confocal micrograph of the conjunctiva of the indicated mice stained with anti-CD4 (blue), anti-B220 (green), and anti-β-III tubulin (red). Scale bars, 100 μm. n = 6 mice per group from 2 independent experiments.
(I) Axon length per area of nictitating membrane of the same sample analyzed in (H). Data represent the mean ± SD. p values were calculated by a one-way analysis of variance (ANOVA) (C, E, F, and I) or two-way analysis of variance (G). ns, not significant.
See also Figure S3.

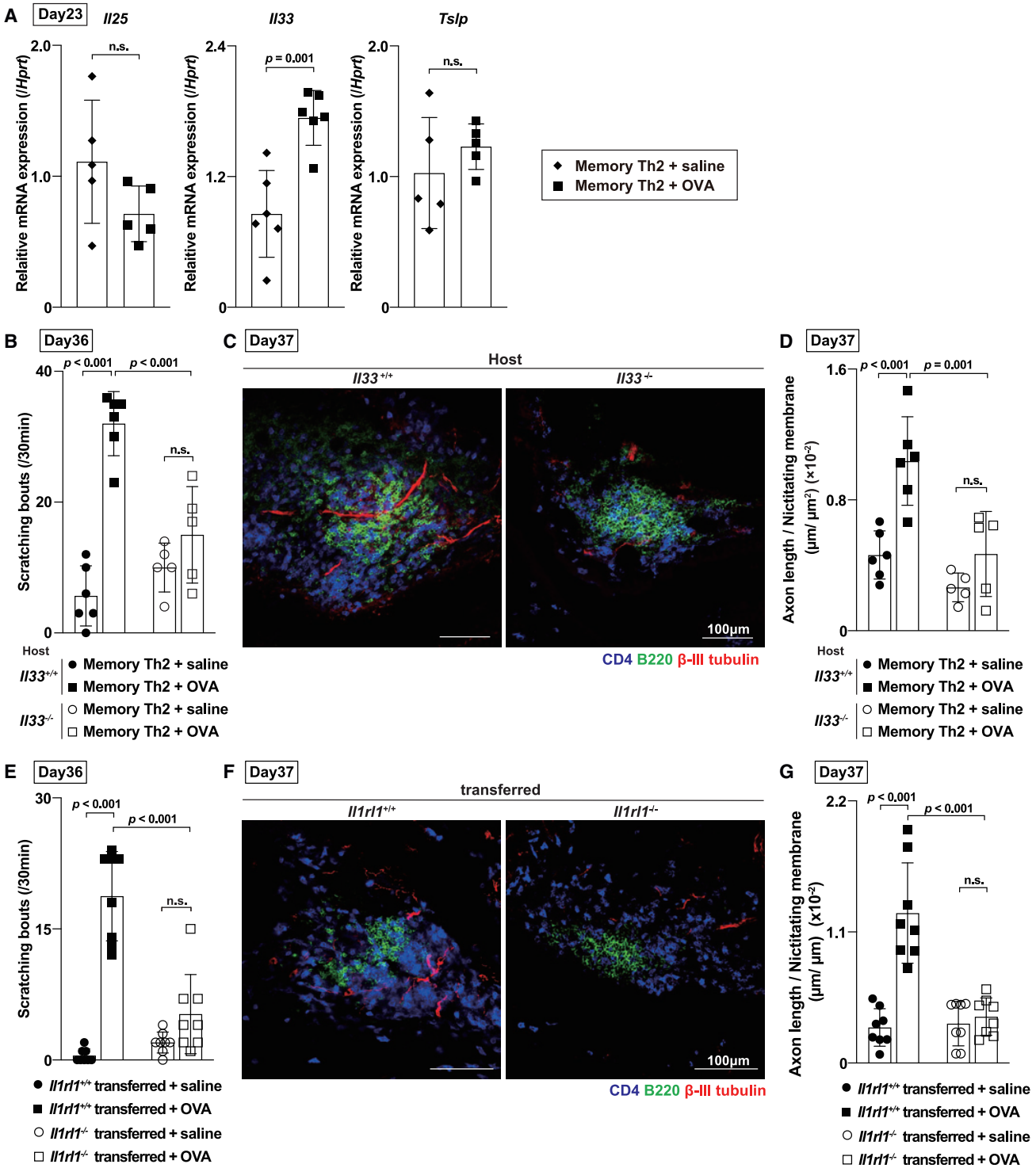

Figure 4. IL-33 regulated severe itch and peripheral nerve elongation in allergic conjunctivitis

(A) Quantitative RT-PCR of *Il25, Il33* and *Tslp* in the conjunctiva from memory Th2-cell-transferred mice treated with saline (memory Th2 + saline) or treated with OVA (memory Th2 + OVA) on day 23. Average of two independent experiments (*Il25* and *Tslp*, n = 5 per group; *Il33*, n = 6 per group).

(B–D) OVA-specific memory Th2 cells were transferred intravenously into Il33$^{+/+}$ and Il33$^{-/-}$ mice that were subsequently treated with OVA, as indicated in Figure S4A.

(B) Absolute number of scratching bouts in memory Th2 cell-transferred Il33$^{+/+}$ mice treated with saline (memory Th2 + saline) or treated with OVA (memory Th2 + OVA) and memory Th2 cell-transferred Il33$^{-/-}$ mice treated with saline (memory Th2 + saline) or treated with OVA (memory Th2 + OVA) (Il33$^{+/+}$ n = 6 per group; and Il33$^{-/-}$, n = 5 per group) from 2 independent experiments.

(legend continued on next page)

conjunctiva of mice that had been immunized with HDM antigen and HP-β-CD, followed by repeated exposure to HDM antigen for three weeks (Huang et al., 2018) (Figure S6A). Retrograde labeling revealed that WGA-positive cells were detected in the TG but not in the dorsal root ganglions (DRGs), indicating that elongated nerves come from the TG (Figures 6A and 6B). At the same time, histological staining of the inflamed conjunctiva revealed that elongated nerves were c-fibers because of the colocalization of peripherin and β-III tubulin (Wainger et al., 2015) (Figure 6C).

We then assessed the characteristics of neurons in the inflamed conjunctiva. To this end, we performed scRNA-seq using the neurons in the TG of HDM-treated mice on day 47. We identified 10 clusters in an unbiased manner based on differentially expressed genes and inferred cluster identities based on the expression of marker genes (Figures 6D and S6B). Among these 10 clusters, clusters 1 to 3 specifically expressed *Trpv1* and *Trpa1*, which are well-known itch-related receptors (Lay and Dong, 2020) (Figure S6B). These three clusters expressed both *Ramp1* and *Calcrl* (Figures 6E and 6F). *Mrgpra3* and *Il31ra* were selectively expressed in part of cluster 2 (Figure 6G). *Il4ra* was expressed in cluster 1 and part of cluster 2, in which *Il31ra* was not expressed, while *Il13ra1* was broadly expressed among the three clusters (Figure 6G). Furthermore, *Sst* was also expressed in cluster 2 (Figure 6G). In contrast, the majority of *Calca*-expressing cells were in cluster 1 (Figure 6G). Furthermore, each cluster showed distinct expression pattern of itch-related genes (Figure 6H). These results indicate that nerves that express *Ramp1* and *Calcrl* also express various types of itch-promoting molecules, including *Trpv1* and *Trpa1*.

We next investigated the pathological roles of CGRP-related receptors in the induction of severe itch. Treatment with BMS-927711, a CGRP receptor antagonist, significantly inhibited HDM exposure-induced itch *in vivo* (Lipton et al., 2019) (Figures S6C and 6I), whereas inhibition of CGRP signaling showed only a slight influence on both axonal elongation and the infiltration of inflammatory cells (Figures S6D and S6E). Administration of BMS-927711 also ameliorated OVA-exposure-induced itch with slight effects on axonal elongation and the infiltration of inflammatory cells *in vivo* (Figures S6F–S6I). Furthermore, *Ramp1*-deficient mice reconstituted with wild-type bone marrow showed a significant decrease in scratching bouts compared with wild-type mice reconstituted with wild-type bone marrow or *Ramp1*-deficient bone marrow (Figures S6J and 6J). However, *Ramp1*-deficient mice reconstituted with wild-type bone marrow showed a small decrease in axonal elongation (Figure S6K). These results indicate that *Ramp1* expression on non-immune cells is important for the induction of severe itch. Furthermore, histological analysis revealed that Ramp1 was expressed and colocalized with beta-III tubulin-positive nerves in the inflamed conjunctiva in wild-type mice reconstituted with wild-type bone marrow (Figure S6L upper panel) but not *Ramp1*-deficient mice reconstituted with wild-type bone marrow (Figure S6L lower panel).

Giant papillae from patients with severe allergic conjunctivitis exhibit axonal elongation together with the formation of CALT structures

Finally, we wanted to determine whether the cellular and molecular mechanisms observed in our animal models were involved in shaping the pathogenesis of severe itch in human chronic allergic conjunctivitis (Table S2). The infiltration of inflammatory cells was observed in giant papillae from patients with severe allergic conjunctivitis but not in the conjunctival mucosa from healthy controls (Figure S7A). The CALT structure containing $CD4^+$ T cells and $CD19^+$ B cells was induced in the giant papillae from patients with severe chronic allergic conjunctivitis, but not in the normal conjunctival mucosa tissue (Figure 7A). The majority of infiltrating $CD4^+$ T cells were $CD45RO^+$ memory-type T cells (Figure 7B). The enhanced expression of IL-33 was detected in the giant papillae from the patients with severe chronic allergic conjunctivitis in comparison with normal conjunctival mucosa tissue (Figure 7C). Importantly, the elongation of nerve fibers was detected by Bielschowsky's silver staining in the giant papillae from patients with severe chronic allergic conjunctivitis, but not in normal conjunctival mucosa tissue (Figure 7D). Histological analyses of the giant papillae also revealed the elongation of the peripheral nerves, which were stained by CD56, Chromogranin, S100, and Synaptosin (Figure S7B). Electron microscopy confirmed the axonal elongation in the giant papillae from patients with severe chronic allergic conjunctivitis (Figure 7E). The CGRP-producing cells infiltrated the giant papillae in patients with severe chronic allergic conjunctivitis, but not the normal conjunctival mucosa tissue (Figure S7C). Histological analyses of the giant papillae revealed $CD4^+$ T cell infiltration in association with the expression of CGRP (Figure 7F). scRNA-seq datasets from the patients with VKC revealed that the $CD4^+$ T cells that had infiltrated the giant papillae included various T cell subsets, such as regulatory T (Treg) cells, Th2 cells, and Th17 cells (Figures 7G and S7D). The Th2 cell population in the giant papillae showed the enhanced expression of *PTGDR2*, *KLRB1*, *IL1RL1*, *IL17RB*, and *HPGDS*, accompanied by inflammatory

(C) A representative confocal micrograph of the conjunctiva stained with anti-CD4 (blue), anti-B220 (green), and anti-β-III tubulin (red) from the indicated mice ($Il33^{+/+}$, n = 6 per group; and $Il33^{-/-}$, n = 5 per group) from 2 independent experiments. Scale bars, 100 μm.
(D) Axon length per area of nictitating membrane of the same sample analyzed in (C).
(E–G) OVA-specific memory Th2 cells derived from $Il1rl1^{+/+}$ and $Il1rl1^{-/-}$ mice were transferred intravenously into BALB/c mice that were subsequently treated with OVA, as indicated in Figure S4F.
(E) Absolute number of scratching bouts in $Il1rl1^{+/+}$ memory Th2 cell-transferred mice treated with saline ($Il1rl1^{+/+}$ transferred + saline) or treated with OVA ($Il1rl1^{+/+}$ transferred + OVA) and $Il1rl1^{-/-}$ memory Th2 cell-transferred mice treated with saline ($Il1rl1^{-/-}$ transferred + saline) or treated with OVA ($Il1rl1^{-/-}$ transferred + OVA). n = 8 mice per group) from 2 independent experiments.
(F) A representative confocal micrograph of the conjunctiva stained with anti-CD4 (blue), anti-B220 (green), and anti-β-III tubulin (red) from the indicated mice. Scale bars, 100 μm. n = 8 mice per group from 2 independent experiments.
(G) Axon length per area of nictitating membrane of the same sample analyzed in (F). Data represent the mean ± SD. p values were calculated by an unpaired t test (A) or a one-way analysis of variance (B, D, E, and G). ns, not significant.
See also Figure S4.

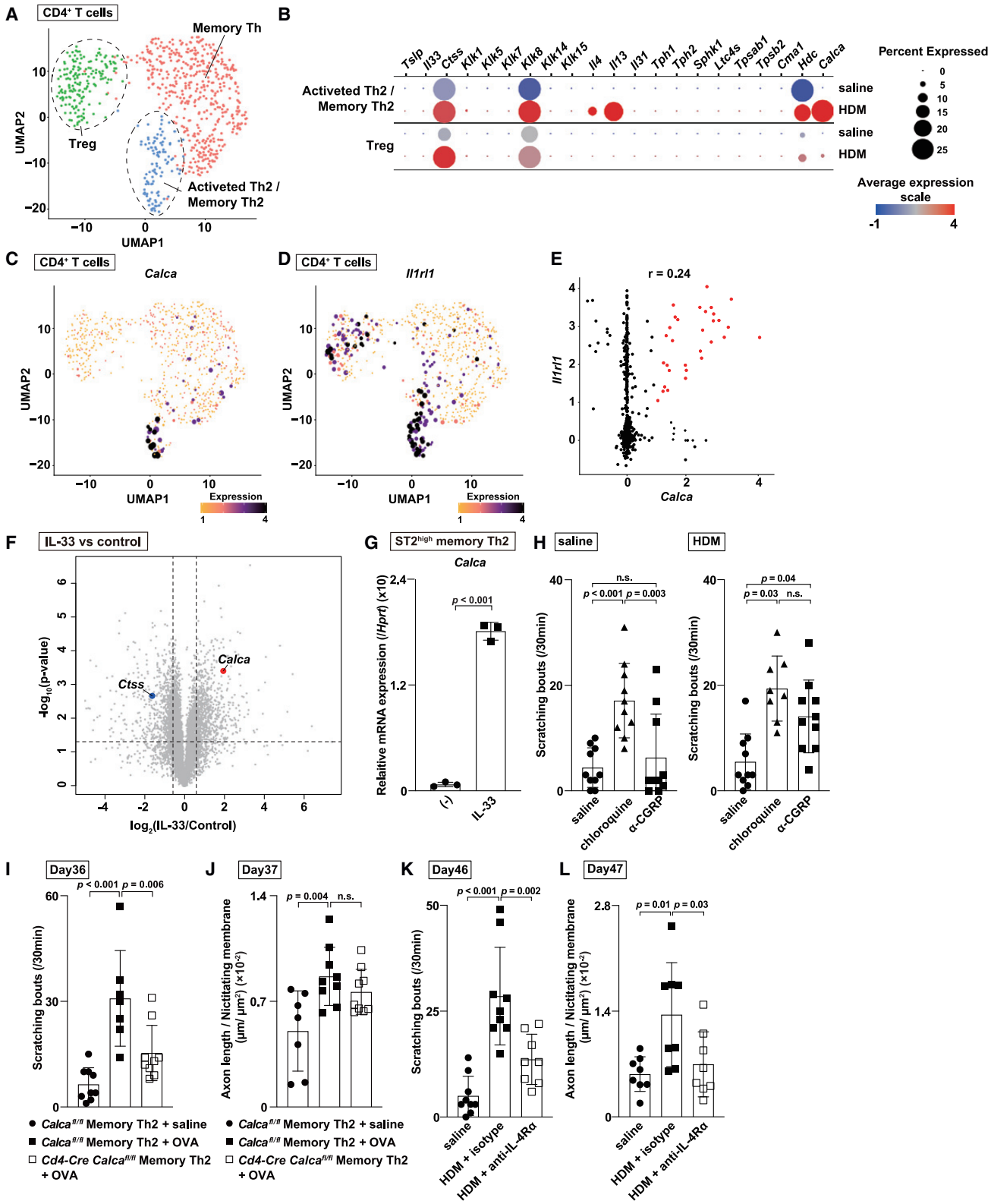

Figure 5. IL-33 stimulation induced the expression of *Calca* by ST2^{hi} memory Th2 cells

(A) A UMAP projection of CD4$^+$ T cells selected from the original dataset (Figure 2A), colored according to cellular subset.

(B) A dot plot of itch-related genes for the indicated cell types. The dot size represented the fraction of cells within the cell type expressing an indicated gene, and the color intensity represented the average mRNA expression of an indicated gene across all cells.

(legend continued on next page)

cytokines (Figures S7E and S7F). Furthermore, *IL1RL1*-expressing CD4$^+$ T cells selectively expressed *CALCA* (Figure 7H). These results indicate that the giant papillae from patients with severe allergic conjunctivitis exhibited axonal elongation together with the accumulation of CGRP-producing *IL1RL1*-positive CD4$^+$ T cells.

DISCUSSION

We identified memory-type pathogenic Th2 cells that regulate severe itch together with neuro-reconstruction during allergic conjunctival inflammation. *Calca*-expressing memory-type pathogenic Th2 cells were identified in the HDM-induced inflamed conjunctiva by a single-cell transcriptomic analysis. We found that IL-33 stimulation induced the expression of *Calca* in ST2^{hi} memory Th2 cells. The genetic deletion of *Il33* or *Il1rl1*, or the pharmacological blockade of CGRP signaling attenuated the frequency of scratching bouts *in vivo*. At the same time, the genetic deletion of *Il33* or *Il1rl1* led to decreased axonal elongation. Thus, the IL-33-ST2 axis controls the expression of *Calca* in memory Th2 cells and the pathogenesis of severe itch. Furthermore, we found that the giant papillae of patients with severe conjunctivitis showed peripheral nerve elongation accompanied by the formation of CALT structures that contained CD45RO$^+$ memory-type CD4$^+$ T cells.

Regarding peripheral nerve elongation, the cellular and molecular mechanisms at the developmental stage have been well studied (Markus et al., 2002). The neurotrophin family members, including nerve growth factor (NGF), are crucial for the development of peripheral nerves (Tucker et al., 2001). NGF also induced peripheral nerve elongation during conditions associated with chronic inflammation (e.g., irritable bowel syndrome and atopic dermatitis) (Dothel et al., 2015; Tominaga and Takamori, 2014). In contrast, the involvement of immune cells in the pathogenesis of peripheral nerve elongation during chronic inflammation remains unclear. In this study, we found that both IL-33 deletion and CD4$^+$ T-cell-specific deletion of ST2 resulted in significant decreased axonal elongation in the inflamed conjunctiva. Furthermore, blockade of IL-4 receptor α signaling also induced significant decreased of axonal elongation. These results clearly show that CD4$^+$ T cells activated via the IL-33-ST2 axis and inflammatory type 2 cytokines, such as IL-4 and IL-13, play a key role in peripheral nerve elongation during chronic allergic inflammation. Our experiments revealed that the elongated nerves in the inflamed conjunctiva include peripherin-positive sensory nerves and come from the TG. Interestingly, the scRNA-dataset of the TG from HDM-exposed mice identified *Il4ra*-expressed neurons, underscoring the important roles of IL-4 and IL-13 in itch-related pathology in chronic conjunctivitis. At the same time, we detected *Mrgpra3*-positive neurons, which are well-investigated pruriceptive receptors neurons, in the TGs of HDM-exposed mice (Huang et al., 2018). Indeed, the administration of chloroquine caused severe itch in our experimental model of HDM exposure (Figure 5H). Furthermore, our results of scRNA-seq dataset analyses of the TG from HDM-exposed mice indicate that *Mrgpra3* and other itch-related receptors, such as *Ramp1* and *Calcrl*, are important for the induction of severe itch in the conjunctiva.

Neural regulation of immunity is crucial for maintaining tissue homeostasis (Chu et al., 2020; Huh and Veiga-Fernandes, 2020; Ordovas-Montanes et al., 2015). For example, sympathetic neurons inhibit type 2 immune responses by regulating type 2 innate lymphoid cells (ILC2s) that express β_2-adrenergic receptors in the intestine (Moriyama et al., 2018). Nociceptive neurons drive the allergic skin inflammation by inducing mast cell degradation via substance P (Serhan et al., 2019). The vagal sensory afferents tune the number of peripheral regulatory T cells and maintain gut homeostasis (Teratani et al., 2020). In the case of bacterial infection, nociceptive neurons suppress the infiltration of neutrophils into the region of local infection via CGRP (Pinho-Ribeiro

(C) The expression of *Calca* projected onto a UMAP.
(D) The expression of *Il1rl1* projected onto a UMAP.
(E) Scatter plots represent Pearson's correlation between the expression of *Calca* and *Il1rl1* in conjunctiva-infiltrating CD4$^+$ T cells from the scRNA-seq dataset.
(F) OVA-specific ST2^{hi} memory Th2 cells were cultured with or without IL-33 for 72 h (Figure S5B). RNA-seq data were computed as fragments per kilobase of transcript per million mapped reads (GEO: GSE114921). The volcano plot depicted the differential gene expression induced by IL-33 in comparison with control.
(G) Quantitative RT-PCR to detect *Calca* in ST2^{hi} memory Th2 cells with or without IL-33 stimulation. n = 3 mice per group from 1 experiment.
(H) Chloroquine or α-CGRP was administered to BALB/c mice after repeated exposure to saline or HDM, as indicated in Figure S5C. The absolute number of scratching bouts among mice exposed to saline (saline), chloroquine diphosphate salt (chloroquine), or α-CGRP trifluoroacetate salt (α-CGRP) on day 46 in the saline-treated mice (n = 9 mice per group from 2 independent experiments) (left) and HDM-treated mice (saline, n = 10; chloroquine, n = 8; α-CGRP, n = 10 from 2 independent experiments) (right).
(I and J) OVA-specific memory Th2 cells derived from *Calca*$^{fl/fl}$ and *CD4-Cre Calca*$^{fl/fl}$ mice were transferred intravenously into BALB/c mice that were subsequently treated with OVA, as indicated in Figure S5E.
(I) Absolute number of scratching bouts in *Calca*$^{fl/fl}$ memory Th2 cell-transferred mice treated with saline (*Calca*$^{fl/fl}$ memory Th2 + saline, n = 9) or treated with OVA (*Calca*$^{fl/fl}$ memory Th2 + OVA, n = 7) or *Cd4-Cre Calca*$^{fl/fl}$ memory Th2 cell-transferred mice treated with OVA (*Cd4-Cre Calca*$^{fl/fl}$ memory Th2 + OVA, n = 9 mice) from 2 independent experiments.
(J) Axon length per area of nictitating membrane of the confocal micrograph of the same sample analyzed in Figure S5F (*Calca*$^{fl/fl}$ memory Th2 + saline, n = 7; *Calca*$^{fl/fl}$ memory Th2 + OVA, n = 9; *Cd4-Cre Calca*$^{fl/fl}$ memory Th2 + OVA, n = 9 from 2 independent experiments).
(K and L) BALB/c mice were treated with saline (saline), HDM with administration of isotype control antibody (HDM + isotype), or HDM with administration of anti-IL-4Rα antibody (HDM + anti-IL-4Rα).
(K) Absolute number of scratching bouts among the indicated mice. n = 9 mice (saline), n = 9 mice (HDM + isotype), and n = 8 mice (HDM + anti-IL-4Rα) from 2 independent experiments.
(L) Axon length per area of nictitating membrane of the confocal micrograph of the same sample analyzed in Figure S5H (n = 8 mice per group from 2 independent experiments). Data represent the mean ± SD. p values were calculated by an unpaired t test (G), or a one-way analysis of variance (H, I, J, K, and L). ns, not significant.
See also Figure S5 and Table S1.

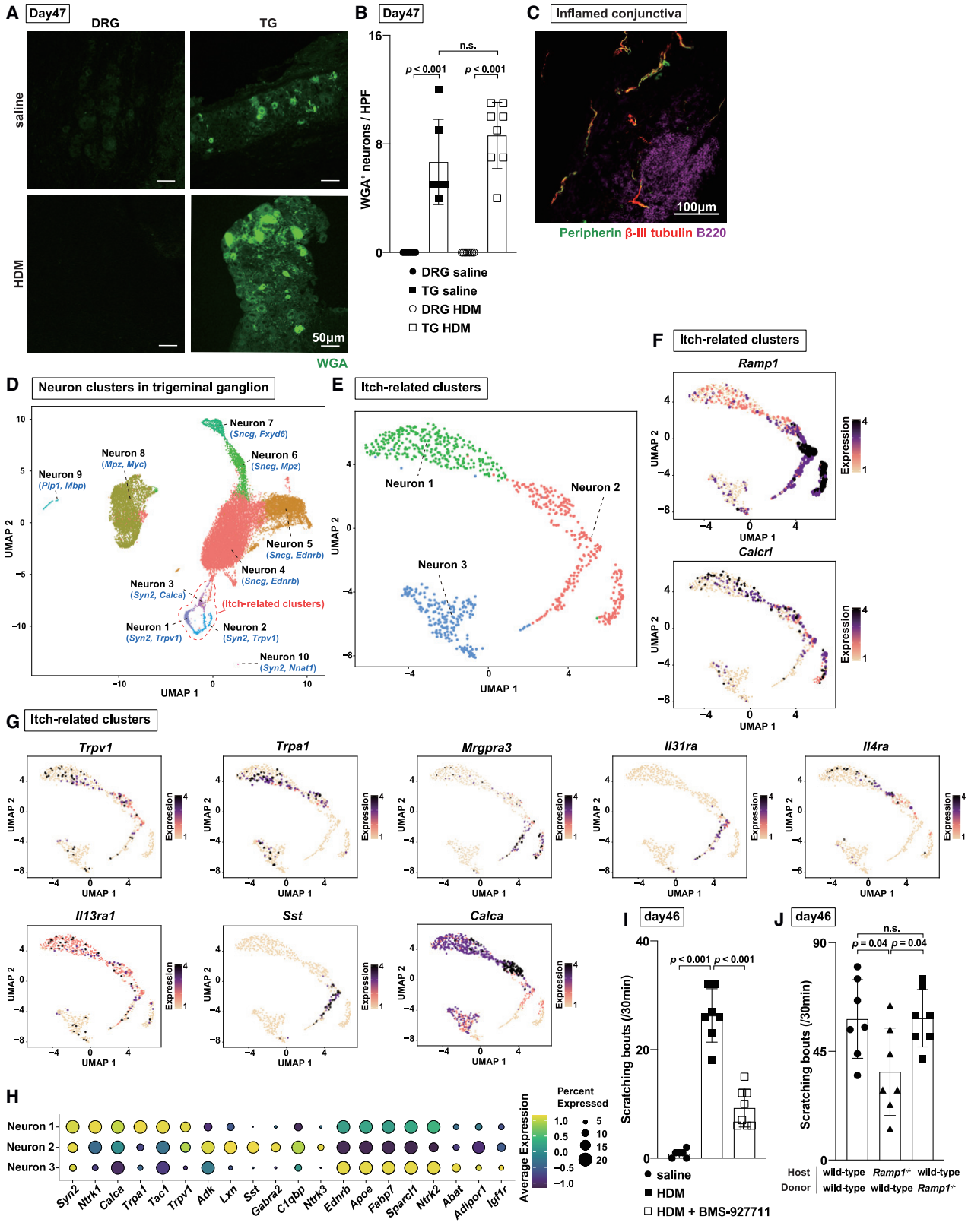

(legend on next page)

et al., 2018). In contrast, in the immunological regulation of neural systems, IL-4 and IL-13 (type 2 cytokines), directly stimulate sensory neurons to induce itch via the IL-4Rα-JAK1 axis (Oetjen et al., 2017). IL-31, which is produced by Th2 cells or conventional type 2 dendritic cells, also induces itch at sites of inflammation (Xu et al., 2020; Yamamura et al., 2017). In our study, we found that IL-33-stimulated ST2^{hi} CD4^{+} T cells, which regulate peripheral nerve elongation. Moreover, IL-33 stimulation resulted in the induction of *Calca* in ST2^{hi} memory Th2 cells and the pharmacological blockade of CGRP signaling ameliorated severe itch in our experimental models. Thus, IL-33-stimulated CD4^{+} T cells are involved in shaping both the pathogenesis of severe itch and neuro-reconstruction in the conjunctiva. IL-33 signaling on sensory neurons is reportedly important for the induction of itch in a model of allergic contact dermatitis and in a dry skin mouse model (Liu et al., 2016; Trier et al., 2022). Thus, IL-33 may induce itch by multiple cellular pathways.

CGRP is a 37-amino-acid neuropeptide that is a potential mediator of the nociceptor neuron function (Rosenfeld et al., 1983; Russell et al., 2014). CGRP-expressing sensory neurons respond to itch stimulation, and genetic deletion of CGRP-expressing sensory neurons results in decreased sensitivity to histamine- and chloroquine-induced itch, suggesting that CGRP is also involved in itch (McCoy et al., 2012, 2013). A number of recent studies have revealed that CGRP plays an important role in the neuro-immune interaction. In the lung, CGRP constrains type 2 inflammation by negatively regulating ILC2 responses (Nagashima et al., 2019; Wallrapp et al., 2019). In the gut, nociceptive neurons regulate M cells via CGRP to control Salmonella infection (Lai et al., 2020). These previous reports indicate that the nervous system regulates the immune system through CGRP. In contrast, our results highlight that CGRP derived from the cells in the immune system regulate the nervous system function. Indeed, our scRNA-seq analysis revealed the induction of *Calca*-expressing memory CD4^{+} T cells in the inflamed conjunctivae during chronic allergic inflammation. The trigeminal ganglion that controls the perception of the conjunctiva expressed receptors of CGRP. A CGRP receptor antagonist ameliorated HDM- and OVA-exposure-induced itch in the conjunctivae in our experimental model. While the details are still unclear, it is possible that pharmacological blockade of CGRP also inhibits the spinal itch transmission in which CGRP play a substantial role. However, the mice that were adoptively transferred with *Calca*-deficient memory Th2 cells showed the significant amelioration of scratching bouts. Thus, the allergen-induced production of CGRP by memory-type pathogenic CD4^{+} T cells also plays an important role in the pathogenesis of severe itch under inflammatory conditions.

The conjunctiva is a unique mucosal tissue that lines the anterior part of the sclera and which is often involved in allergic inflammation because it is the mucosal tissue that is most accessible to various airborne allergens (e.g., pollen, house dust mite, and animal dander) (Elieh Ali Komi et al., 2018; Leibowitz, 2000). The giant papillae in patients with severe chronic allergic conjunctivitis show the enhanced expression of IL-33 (Matsuda et al., 2009), and the massive infiltration of effector Th2 cells and memory-type CD45RO^{+}CD4^{+} T cells in inflamed conjunctival tissue from patients with chronic allergic conjunctivitis has been reported (Leibowitz, 2000). We confirmed the upregulation of IL-33 in the inflammatory giant papillae. Moreover, we found that infiltrating memory-type CD4^{+} T cells contain *Calca*-expressing pathogenic CD4^{+} T cells that induce severe itch in the conjunctivae.

Various subpopulations of pathogenic Th2 cells shape the pathogenesis of type 2 inflammation in both humans and mice (Morimoto et al., 2018; Nakayama et al., 2017; Ruterbusch et al., 2020; Wambre et al., 2017). Pathogenic memory Th2 cells producing high amounts of IL-5 play an important role in shaping the pathogenesis of eosinophilic inflammation (Endo et al., 2015; Nakayama et al., 2017). Another population of pathogenic memory Th2 cells that produce amphiregulin induce a fibrotic response during eosinophilic inflammation (Morimoto et al., 2018). Interestingly, both subpopulations of pathogenic

Figure 6. Sensory neurons of inflamed trigeminal ganglion expressed various itch-promoting molecules

(A and B) Retrograde labeling was performed, followed by repeated exposure to HDM as indicated in Figure S6A.

(A) A representative confocal micrograph of dorsal root ganglion (DRG) and trigeminal ganglion (TG), stained retrogradely with WGA, from the indicated mice. Scale bars, 50 μm. n = 6 mice treated with saline and n = 8 treated with HDM from 2 independent experiments.

(B) Absolute number of WGA^{+} cells per high-power field of the micrograph in DRG or TG of the mice treated with saline (DRG saline, TG saline, n = 6 mice per group) or the mice treated with HDM (DRG HDM, TG HDM, n = 8 mice per group) from 2 independent experiments.

(C) A representative confocal micrograph of the conjunctiva stained with anti-peripherin (green), anti-β-III tubulin (red), and anti-B220 (magenta) from mice treated with HDM on day 47. Scale bars, 100 μm. n = 3 mice from 1 experiment.

(D–H) CD45^{-}CD31^{-}EpCAM^{-} cells from trigeminal ganglia of mice treated with HDM were analyzed by scRNA-seq. n = 9 mice per group from 2 independents experiments.

(D) Ten gene expression clusters (0–10) projected on a UMAP of the scRNA-seq libraries from the trigeminal ganglion of mice treated with HDM on day 47, as indicated in Figure S1A, and colored according to the cellular subset.

(E) A UMAP projection of clusters 1 to 3 as "itch-related clusters" selected from the original dataset highlighting the cellular source of mice treated with HDM, colored according to the cellular subset.

(F) The expression of *Ramp1* (upper panel) and *Calcrl* (lower panel) projected onto a UMAP.

(G) The expression of *Trpv1*, *Trpa1*, *Mrgpra3*, *Il31ra*, and *Il4ra* (from left in the upper row), and *Il13ra1*, *Sst*, and *Calca* (from left in the lower row) projected onto a UMAP, respectively.

(H) A dot plot of 20 genes for the indicated cell types. The dot size represented the fraction of cells within the cell type expressing an indicated gene, and the color intensity represented the average expression of an indicated gene across all cells.

(I) Absolute number of scratching bouts in mice treated with saline (saline), HDM exposure (HDM), or HDM exposure together with BMS-927711 treatment (HDM + BMS-927711) (n = 8 mice per group), as indicated in Figure S6C. n = 8 mice per group from 2 independent experiments.

(J) Absolute number of scratching bouts in the indicated mice (n = 7 mice per group from 2 independent experiments) treated with HDM. Data represent the mean ± SD. p values were calculated by a one-way analysis of variance (B, I, and J). ns, not significant.

See also Figure S6.

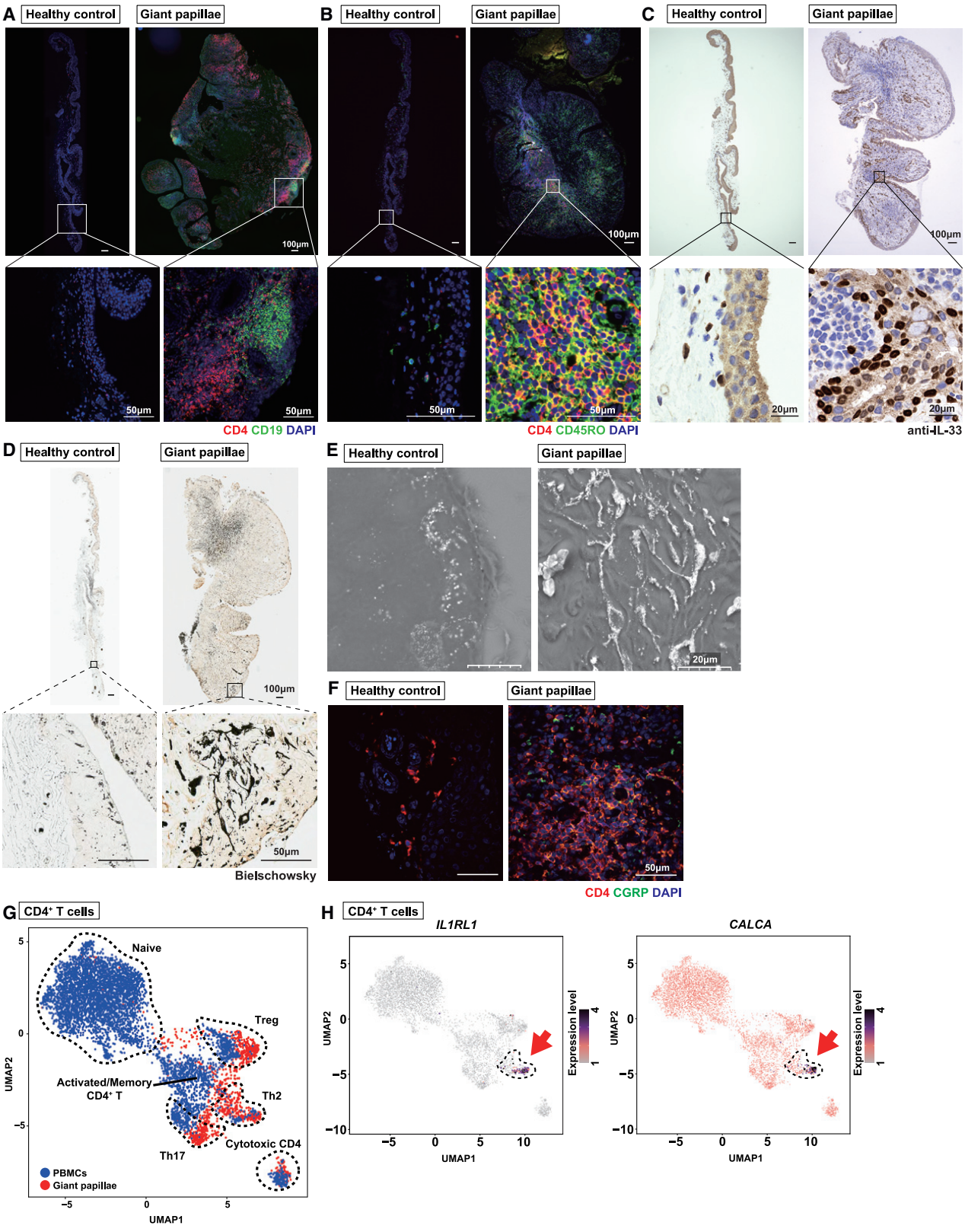

(legend on next page)

memory Th2 cells are induced by IL-33 stimulation. In the case of allergic conjunctivitis, we demonstrated that the IL-33-ST2 axis regulated neuro-reconstruction by inducing the expression of *Calca* in memory-type pathogenic Th2 cells.

In summary, we investigated experimental mouse models of allergic conjunctival inflammation and examined the giant papillae of patients with allergic conjunctivitis. We identified that the IL-33-ST2 axis in memory-type pathogenic Th2 cells regulated scratching bouts and peripheral nerve elongation in the chronically inflamed conjunctival tissue with the formation of CALT structure. We also found that the *Calca* expressed by memory-type pathogenic Th2 cells controlled severe itch. Understanding the cellular and molecular mechanisms through which the pathology of neuro-immune mediated diseases is shaped will be essential for the development of new therapeutic strategies for intractable inflammatory diseases.

Limitations of the study

Regarding the effects of CGRP on neurons, our results revealed the expression of Ramp1 on peripheral neurons in the inflamed conjunctiva, which suggests that CGRP affects these peripheral neurons directly. However, CGRP may induce the itch also by activating infiltrated inflammatory cells. Indeed, it is reported that Mas-related G-protein-coupled receptor-X2 (MRGPRX2; mouse counterpart MrgprB2)-expressed mast cells are involved in the induction of non-histaminergic itch and mast-cell-dependent inflammation (Meixiong et al., 2019; Serhan et al., 2019). Further investigation will be needed to determine whether the immune cells such as MRGPRX2-expressing mast cells are involved in the pruritogenic effects of CGRP.

STAR★METHODS

Detailed methods are provided in the online version of this paper and include the following:

SUPPLEMENTAL INFORMATION

Supplemental information can be found online at https://doi.org/10.1016/j.immuni.2022.09.016.

ACKNOWLEDGMENTS

We thank Dr. Tetsuichiro Saito for his helpful discussion; Drs. Satoru Takahashi and Seiya Mizuno for their valuable contributions concerning the

Figure 7. Giant papillae from patients with severe allergic conjunctivitis showed axonal elongation accompanied by CGRP-producing memory-type CD4$^+$ T cells

(A) A representative confocal micrograph of the conjunctival mucosa from a healthy control subject (left) and giant papillae from a patient with severe allergic conjunctivitis (right) stained with anti-CD4 (red), anti-CD19 (green), and 4',6-diamidino-2-phenylindole (DAPI) (blue). Scale bars, 100 μm (upper panels) and 50 μm (lower panels).

(B) A representative confocal micrograph of the conjunctival mucosa from a healthy control subject (left) and giant papillae from a patient with severe allergic conjunctivitis (right) stained with anti-CD4 (red), anti-CD45RO (green), and anti-DAPI (blue). Scale bars, 100 μm (upper panels) and 50 μm (lower panels).

(C) A representative confocal micrograph of the conjunctival mucosa from a healthy control subject (left) and giant papillae from a patient with severe allergic conjunctivitis (right) stained with anti-IL-33. Scale bars, 100 μm (upper panels) and 20 μm (lower panels).

(D) A representative confocal micrograph of the conjunctival mucosa from a healthy control subject (left) and giant papillae from a patient with severe allergic conjunctivitis (right) stained with Bieschowsky. Scale bars, 100 μm (upper panels) and 50 μm (lower panels).

(E) A representative electron micrograph of the conjunctival mucosa from a healthy control subject (left) and giant papillae from a patient with severe allergic conjunctivitis (right) (Bielschowsky's silver staining). Scale bars, 20 μm.

(F) A representative confocal micrograph of the conjunctival mucosa from a healthy control subject (left) and giant papillae from a patient with severe allergic conjunctivitis (right) stained with anti-CD4 (red), anti-CGRP (green), and DAPI (blue). Scale bars, 50 μm.

(G) CD45$^+$ cells were isolated by FACS from the conjunctival tissue (Giant papillae) or peripheral blood mononuclear cells (PBMCs) of VKC patients and analyzed by scRNA-seq. A UMAP projection of CD4$^+$ cells selected from the original dataset, colored according to the cellular subset.

(H) The expression of *IL1RL1* (left) and *CALCA* (right) projected onto a UMAP. The red arrow refers to the cluster that specifically expresses the genes on each UMAP. (A and B) n = 1 (healthy control) and n = 4 (giant papillae); (C–F) n = 1 (healthy control) and n = 3 (giant papillae); and (G and H) PBMCs and giant papillae from 1 patient.

See also Figure S7 and Table S2.

production of *Calca* flox mice; and Toshihiro Ito, Kaoru Sugaya, and Kazuhiko Azuma for their excellent technical assistance. This work was supported by the following grants: Ministry of Education, Culture, Sports, Science and Technology(MEXT Japan) Grants-in-Aid for Scientific Research (S) 26221305, JP19H05650, (B) 20H03685, (C) 17K08876, 18K07164, and 19K16683, Transformative Research Areas (B) JP21H05120; Practical Research Project for Allergic Diseases and Immunology (Research on Allergic Diseases and Immunology) from the Japan Agency for Medical Research and Development, AMED (Nos. JP20ek0410060 and JP22ek0410092); AMED-PRIME, AMED (No. JP20gm6110005); AMED-CREST, AMED (No. JP20gm1210003); JST FOREST Project(No. JPMJFR200R); JST-Moonshot R&D (No. JPMJMS2025); SENTAN project (JP19hm0102069h001); Mochida Memorial Foundation for Medical and Pharmaceutical Research, MSD Life Science Foundation, The Naito Foundation and Takeda Science Foundation.

AUTHOR CONTRIBUTIONS

M. Oka, K.H., M.K., and T.N. designed the experiments. M. Oka., K.H., M.K., M. Ono., C.I., K.K., T.H., and Y.M. performed the experiments. M. Oka., K.H., M.K., M. Ono., Y.I., A.M., N.E., and T.N. analyzed and interpreted the data. M. Oka., K.H., and T.N. wrote the paper.

DECLARATION OF INTERESTS

The authors declare no competing interests.

Received: May 22, 2022
Revised: August 8, 2022
Accepted: September 28, 2022
Published: October 21, 2022

REFERENCES

Azari, A.A., and Barney, N.P. (2013). Conjunctivitis: a systematic review of diagnosis and treatment. JAMA *310*, 1721–1729.

Chu, C., Artis, D., and Chiu, I.M. (2020). Neuro-immune interactions in the tissues. Immunity *52*, 464–474.

Dothel, G., Barbaro, M.R., Boudin, H., Vasina, V., Cremon, C., Gargano, L., Bellacosa, L., De Giorgio, R., Le Berre-Scoul, C., Aubert, P., et al. (2015). Nerve fiber outgrowth is increased in the intestinal mucosa of patients with irritable bowel syndrome. Gastroenterology *148*, 1002–1011.e4.

Elieh Ali Komi, D., Rambasek, T., and Bielory, L. (2018). Clinical implications of mast cell involvement in allergic conjunctivitis. Allergy *73*, 528–539.

Endo, Y., Hirahara, K., Iinuma, T., Shinoda, K., Tumes, D.J., Asou, H.K., Matsugae, N., Obata-Ninomiya, K., Yamamoto, H., Motohashi, S., et al. (2015). The interleukin-33-p38 kinase axis confers memory T helper 2 cell pathogenicity in the airway. Immunity *42*, 294–308.

Hirahara, K., Yamashita, M., Iwamura, C., Shinoda, K., Hasegawa, A., Yoshizawa, H., Koseki, H., Gejyo, F., and Nakayama, T. (2008). Repressor of GATA regulates TH2-driven allergic airway inflammation and airway hyperresponsiveness. J. Allergy Clin. Immunol. *122* 512–20, e11.

Huang, C.C., Yang, W., Guo, C., Jiang, H., Li, F., Xiao, M., Davidson, S., Yu, G., Duan, B., Huang, T., et al. (2018). Anatomical and functional dichotomy of ocular itch and pain. Nat. Med. *24*, 1268–1276.

Huh, J.R., and Veiga-Fernandes, H. (2020). Neuroimmune circuits in inter-organ communication. Nat. Rev. Immunol. *20*, 217–228.

Ichikawa, T., Hirahara, K., Kokubo, K., Kiuchi, M., Aoki, A., Morimoto, Y., Kumagai, J., Onodera, A., Mato, N., Tumes, D.J., et al. (2019). CD103hi Treg cells constrain lung fibrosis induced by CD103lo tissue-resident pathogenic CD4 T cells. Nat. Immunol. *20*, 1469–1480.

Katzenell, S., Cabrera, J.R., North, B.J., and Leib, D.A. (2017). Isolation, Purification, and Culture of Primary Murine Sensory Neurons. Methods Mol Biol. *1656*, 229–251.

Lai, N.Y., Musser, M.A., Pinho-Ribeiro, F.A., Baral, P., Jacobson, A., Ma, P., Potts, D.E., Chen, Z., Paik, D., Soualhi, S., et al. (2020). Gut-innervating nociceptor neurons regulate Peyer's patch microfold cells and SFB levels to mediate salmonella Host Defense. Cell *180*, 33–49.e22.

Langmead, B., and Salzberg, S.L. (2012). Fast gapped-read alignment with Bowtie 2. Nat Methods. *9*, 357–359.

Lay, M., and Dong, X. (2020). Neural mechanisms of itch. Annu. Rev. Neurosci. *43*, 187–205.

Leibowitz, H.M. (2000). The red eye. N. Engl. J. Med. *343*, 345–351.

Leonardi, A. (2002). Vernal keratoconjunctivitis: pathogenesis and treatment. Prog. Retin. Eye Res. *21*, 319–339.

Li, H., and Durbin, R. (2009). Fast and accurate short read alignment with Burrows-Wheeler transform. Bioinformatics. *25*, 1754–1760.

Lipton, R.B., Croop, R., Stock, E.G., Stock, D.A., Morris, B.A., Frost, M., Dubowchik, G.M., Conway, C.M., Coric, V., and Goadsby, P.J. (2019). Rimegepant, an oral calcitonin gene-related peptide receptor antagonist, for migraine. N. Engl. J. Med. *381*, 142–149.

Liu, B., Tai, Y., Achanta, S., Kaelberer, M.M., Caceres, A.I., Shao, X., Fang, J., and Jordt, S.E. (2016). IL-33/ST2 signaling excites sensory neurons and mediates itch response in a mouse model of poison ivy contact allergy. Proc. Natl. Acad. Sci. USA *113*, E7572–E7579.

Macosko, E.Z., Basu, A., Satija, R., Nemesh, J., Shekhar, K., Goldman, M., Tirosh, I., Bialas, A.R., Kamitaki, N., Martersteck, E.M., et al. (2015). Highly parallel genome-wide expression profiling of individual cells using nanoliter droplets. Cell *161*, 1202–1214.

Manz, R.A., Hauser, A.E., Hiepe, F., and Radbruch, A. (2005). Maintenance of serum antibody levels. Annu. Rev. Immunol. *23*, 367–386.

Markus, A., Patel, T.D., and Snider, W.D. (2002). Neurotrophic factors and axonal growth. Curr. Opin. Neurobiol. *12*, 523–531.

Matsuda, A., Ebihara, N., Yokoi, N., Maruyama, K., Hamuro, J., Kinoshita, S., and Murakami, A. (2010). Lymphoid neogenesis in the giant papillae of patients with chronic allergic conjunctivitis. J. Allergy Clin. Immunol. *126* 1310–2.e1.

Matsuda, A., Okayama, Y., Terai, N., Yokoi, N., Ebihara, N., Tanioka, H., Kawasaki, S., Inatomi, T., Katoh, N., Ueda, E., et al. (2009). The role of interleukin-33 in chronic allergic conjunctivitis. Invest. Ophthalmol. Vis. Sci. *50*, 4646–4652.

McCoy, E.S., Taylor-Blake, B., Street, S.E., Pribisko, A.L., Zheng, J., and Zylka, M.J. (2013). Peptidergic CGRPalpha primary sensory neurons encode heat and itch and tonically suppress sensitivity to cold. Neuron *78*, 138–151.

McCoy, E.S., Taylor-Blake, B., and Zylka, M.J. (2012). CGRPalpha-expressing sensory neurons respond to stimuli that evoke sensations of pain and itch. PLoS One *7*, e36355.

Meixiong, J., Anderson, M., Limjunyawong, N., Sabbagh, M.F., Hu, E., Mack, M.R., Oetjen, L.K., Wang, F., Kim, B.S., and Dong, X. (2019). Activation of mast-cell-expressed Mas-related G-protein-coupled receptors drives non-histaminergic itch. Immunity *50*, 1163–1171.e5.

Mitson-Salazar, A., Yin, Y., Wansley, D.L., Young, M., Bolan, H., Arceo, S., Ho, N., Koh, C., Milner, J.D., Stone, K.D., et al. (2016). Hematopoietic prostaglandin D synthase defines a proeosinophilic pathogenic effector human TH2 cell subpopulation with enhanced function. J. Allergy Clin. Immunol. *137*, 907–918.e9.

Morimoto, Y., Hirahara, K., Kiuchi, M., Wada, T., Ichikawa, T., Kanno, T., Okano, M., Kokubo, K., Onodera, A., Sakurai, D., et al. (2018). Amphiregulin-producing pathogenic memory T helper 2 cells instruct eosinophils to secrete osteopontin and facilitate airway fibrosis. Immunity *49*, 134–150.e6.

Moriyama, S., Brestoff, J.R., Flamar, A.L., Moeller, J.B., Klose, C.S.N., Rankin, L.C., Yudanin, N.A., Monticelli, L.A., Putzel, G.G., Rodewald, H.R., and Artis, D. (2018). beta2-adrenergic receptor-mediated negative regulation of group 2 innate lymphoid cell responses. Science *359*, 1056–1061.

Mortazavi, A., Williams, B.A., McCue, K., Schaeffer, L., and Wold, B. (2008). Mapping and quantifying mammalian transcriptomes by RNA-Seq. Nat Methods. *5*, 621–628.

Nagashima, H., Mahlakõiv, T., Shih, H.Y., Davis, F.P., Meylan, F., Huang, Y., Harrison, O.J., Yao, C., Mikami, Y., Urban, J.F., Jr., et al. (2019). Neuropeptide CGRP limits Group 2 innate lymphoid cell responses and constrains Type 2 inflammation. Immunity *51*, 682–695.e6.

Nakayama, T., Hirahara, K., Onodera, A., Endo, Y., Hosokawa, H., Shinoda, K., Tumes, D.J., and Okamoto, Y. (2017). Th2 cells in health and disease. Annu. Rev. Immunol. *35*, 53–84.

Oboki, K., Ohno, T., Kajiwara, N., Arae, K., Morita, H., Ishii, A., Nambu, A., Abe, T., Kiyonari, H., Matsumoto, K., et al. (2010). IL-33 is a crucial amplifier of innate rather than acquired immunity. Proc. Natl. Acad. Sci. USA *107*, 18581–18586.

Oetjen, L.K., Mack, M.R., Feng, J., Whelan, T.M., Niu, H., Guo, C.J., Chen, S., Trier, A.M., Xu, A.Z., Tripathi, S.V., et al. (2017). Sensory neurons co-opt classical immune signaling pathways to mediate chronic itch. Cell *171*, 217–228.e13.

Ogata, H., Akita, S., Ikehara, S., Azuma, K., Yamaguchi, T., Maimaiti, M., Maezawa, Y., Kubota, Y., Yokote, K., Mitsukawa, N., et al. (2021). Calcification in Werner syndrome associated with lymphatic vessels aging. Aging (Albany, NY) *13*, 25717–25728.

Onishi, M., Ozasa, K., Kobiyama, K., Ohata, K., Kitano, M., Taniguchi, K., Homma, T., Kobayashi, M., Sato, A., Katakai, Y., et al. (2015). Hydroxypropyl-beta-cyclodextrin spikes local inflammation that induces Th2 cell and T follicular helper cell responses to the coadministered antigen. J. Immunol. *194*, 2673–2682.

Ordovas-Montanes, J., Rakoff-Nahoum, S., Huang, S., Riol-Blanco, L., Barreiro, O., and von Andrian, U.H. (2015). The regulation of immunological processes by peripheral neurons in homeostasis and disease. Trends Immunol. *36*, 578–604.

Pinho-Ribeiro, F.A., Baddal, B., Haarsma, R., O'Seaghdha, M., Yang, N.J., Blake, K.J., Portley, M., Verri, W.A., Dale, J.B., Wessels, M.R., and Chiu, I.M. (2018). Blocking neuronal signaling to immune cells treats streptococcal invasive infection. Cell *173*, 1083–1097.e22.

R Development Core Team (2022). CRAN: Manuals. https://cran.r-project.org/manuals.html.

Ram, J., and Agarwal, A. (2014). Images in clinical medicine. Giant papillae in vernal keratoconjunctivitis. N. Engl. J. Med. *370*, 1636.

Rosenfeld, M.G., Mermod, J.J., Amara, S.G., Swanson, L.W., Sawchenko, P.E., Rivier, J., Vale, W.W., and Evans, R.M. (1983). Production of a novel neuropeptide encoded by the calcitonin gene via tissue-specific RNA processing. Nature *304*, 129–135.

Russell, F.A., King, R., Smillie, S.J., Kodji, X., and Brain, S.D. (2014). Calcitonin gene-related peptide: physiology and pathophysiology. Physiol. Rev. *94*, 1099–1142.

Ruterbusch, M., Pruner, K.B., Shehata, L., and Pepper, M. (2020). In vivo CD4+ T cell differentiation and function: revisiting the Th1/Th2 paradigm. Annu. Rev. Immunol. *38*, 705–725.

Sallusto, F., Geginat, J., and Lanzavecchia, A. (2004). Central memory and effector memory T cell subsets: function, generation, and maintenance. Annu. Rev. Immunol. *22*, 745–763.

Serhan, N., Basso, L., Sibilano, R., Petitfils, C., Meixiong, J., Bonnart, C., Reber, L.L., Marichal, T., Starkl, P., Cenac, N., et al. (2019). House dust mites activate nociceptor-mast cell clusters to drive type 2 skin inflammation. Nat. Immunol. *20*, 1435–1443.

Seumois, G., Zapardiel-Gonzalo, J., White, B., Singh, D., Schulten, V., Dillon, M., Hinz, D., Broide, D.H., Sette, A., Peters, B., and Vijayanand, R. (2016). Transcriptional profiling of Th2 cells identifies pathogenic features associated with asthma. J. Immunol. *197*, 655–664.

Shinoda, K., Hirahara, K., Iinuma, T., Ichikawa, T., Suzuki, A.S., Sugaya, K., Tumes, D.J., Yamamoto, H., Hara, T., Tani-ichi, S., et al. (2016). Thy1+IL-7+ lymphatic endothelial cells in iBALT provide a survival niche for memory T-helper cells in allergic airway inflammation. Proc. Natl. Acad. Sci. USA *113*, E2842–E2851.

Stuart, T., Butler, A., Hoffman, P., Hafemeister, C., Papalexi, E., Mauck, W.M., 3rd, Hao, Y., Stoeckius, M., Smibert, P., and Satija, R. (2019). Comprehensive Integration of Single-Cell Data. Cell. *177*, 1888–1902.

Sy, H., and Bielory, L. (2013). Atopic keratoconjunctivitis. Allergy Asthma Proc. *34*, 33–41.

Teratani, T., Mikami, Y., Nakamoto, N., Suzuki, T., Harada, Y., Okabayashi, K., Hagihara, Y., Taniki, N., Kohno, K., Shibata, S., et al. (2020). The liver-brain-gut neural arc maintains the Treg cell niche in the gut. Nature *585*, 591–596.

Tominaga, M., and Takamori, K. (2014). Itch and nerve fibers with special reference to atopic dermatitis: therapeutic implications. J. Dermatol. *41*, 205–212.

Trapnell, C., Pachter, L., and Salzberg, S.L. (2009). TopHat: discovering splice junctions with RNA-Seq. Bioinformatics. *25*, 1105–1111.

Trier, A.M., Mack, M.R., Fredman, A., Tamari, M., Ver Heul, A.M., Zhao, Y., Guo, C.J., Avraham, O., Ford, Z.K., Oetjen, L.K., et al. (2022). IL-33 signaling in sensory neurons promotes dry skin itch. J. Allergy Clin. Immunol. *149*, 1473–1480.e6.

Tucker, K.L., Meyer, M., and Barde, Y.A. (2001). Neurotrophins are required for nerve growth during development. Nat. Neurosci. *4*, 29–37.

Usoskin, D., Furlan, A., Islam, S., Abdo, H., Lönnerberg, P., Lou, D., Hjerling-Leffler, J., Haeggström, J., Kharchenko, O., Kharchenko, P.V., et al. (2015). Unbiased classification of sensory neuron types by large-scale single-cell RNA sequencing. Nat. Neurosci. *18*, 145–153.

Wainger, B.J., Buttermore, E.D., Oliveira, J.T., Mellin, C., Lee, S., Saber, W.A., Wang, A.J., Ichida, J.K., Chiu, I.M., Barrett, L., et al. (2015). Modeling pain in vitro using nociceptor neurons reprogrammed from fibroblasts. Nat. Neurosci. *18*, 17–24.

Wallrapp, A., Burkett, P.R., Riesenfeld, S.J., Kim, S.J., Christian, E., Abdulnour, R.E., Thakore, P.I., Schnell, A., Lambden, C., Herbst, R.H., et al. (2019). Calcitonin gene-related peptide negatively regulates alarmin-driven Type 2 innate lymphoid cell responses. Immunity *51*, 709–723.e6.

Wambre, E., Bajzik, V., DeLong, J.H., O'Brien, K., Nguyen, Q.A., Speake, C., Gersuk, V.H., DeBerg, H.A., Whalen, E., Ni, C., et al. (2017). A phenotypically and functionally distinct human TH2 cell subpopulation is associated with allergic disorders. Sci. Transl. Med. *9*, eaam9171.

Wilson, S.R., Thé, L., Batia, L.M., Beattie, K., Katibah, G.E., McClain, S.P., Pellegrino, M., Estandian, D.M., and Bautista, D.M. (2013). The epithelial cell-derived atopic dermatitis cytokine TSLP activates neurons to induce itch. Cell *155*, 285–295.

Xu, J., Zanvit, P., Hu, L., Tseng, P.Y., Liu, N., Wang, F., Liu, O., Zhang, D., Jin, W., Guo, N., and Fukui, Y. (2020). The cytokine TGF-beta induces interleukin-31 expression from dermal dendritic cells to activate sensory neurons and stimulate wound itching. Immunity *53*, 371–383.e5.

Yamamura, K., Uruno, T., Shiraishi, A., Tanaka, Y., Ushijima, M., Nakahara, T., Watanabe, M., Kido-Nakahara, M., Tsuge, I., Furue, M., and Fukui, Y. (2017). The transcription factor EPAS1 links DOCK8 deficiency to atopic skin inflammation via IL-31 induction. Nat. Commun. *8*, 13946.

Zeisel, A., Hochgerner, H., Lönnerberg, P., Johnsson, A., Memic, F., van der Zwan, J., Häring, M., Braun, E., Borm, L.E., La Manno, G., et al. (2018). Molecular Architecture of the Mouse Nervous System. Cell. *174*, 999–1014.

STAR★METHODS

KEY RESOURCES TABLE

REAGENT or RESOURCE	SOURCE	IDENTIFIER
Antibodies		
APC Rat anti-Mouse CD21/CD35	BD Biosciences	Cat# 561770; RRID: AB_10892818
FITC Rat Anti-Mouse CD90.2	BD Biosciences	Cat# 553004; RRID: AB_394543
PE Rat Anti-Mouse CD45R/B220	BD Biosciences	Cat# 553090; RRID: AB_394620
PE Rat Anti-Mouse Siglec-F	BD Biosciences	Cat# 552126; RRID: AB_394341
Purified Hamster Anti-Mouse CD3e	BD Biosciences	Cat# 553064; RRID: AB_394597
Alexa Flour® 647 anti-mouse CD4 Antibody	BioLegend	Cat# 100530; RRID: AB_389325
Alexa Fluor (R) 488 anti-Tubulin beta 3 (TUBB3) antibody	BioLegend	Cat # 801203; RRID: AB_2564757
APC anti-mouse CD4 Antibody	BioLegend	Cat# 100516; RRID: AB_312719
Brilliant Violet 421™ anti-mouse CD170 (siglec-F) Antibody	BioLegend	Cat# 155509; RRID: AB_2810421
Brilliant Violet 421™ anti-mouse CD4 Antibody	BioLegend	Cat# 100544; RRID: AB_11219790
Brilliant Violet 421™ anti-mouse IL-33Rα (IL1RL1, ST2) Antibody	BioLegend	Cat# 145309; RRID: AB_2565634
FITC anti-mouse CD45 Antibody	BioLegend	Cat# 103107; RRID: AB_312972
FITC anti-mouse Ly6G/Ly6c (Gr-1) Antibody	BioLegend	Cat# 108406; RRID: AB_313371
FITC anti-mouse TCR DO11.10 Antibody	BioLegend	Cat# 118506; RRID: AB_1134180
PE anti-mouse CD4 Antibody	BioLegend	Cat# 100512; RRID: AB_312715
PE anti-mouse IL-33R alpha (IL1RL1, ST2) antibody	BioLegend	Cat # 145304; RRID: AB_2561915
PE/Cyanine7 anti-mouse CD45 Antibody	BioLegend	Cat# 103114; RRID: AB_312979
anti-Beta III Tubulin,Alexa Fluor®488 Conjugate	Merck Millipore	Cat# AB15708A4; RRID: AB_10916541
TCR DO11.10 Monoclonal Antibody (KJ1-26 (KJ126, KJI-26, KJI26)), APC, eBioscience™	Thermo Fisher	Cat# 17-5808-80; RRID: AB_469459
CD31 (PECAM-1) Monoclonal Antibody (390), APC, eBioscience™	Thermo Fisher Scientific	Cat# 17-0311-80; RRID: AB_657736
CD45R (B220) Monoclonal Antibody (RA3-6B2), Alexa Fluor 488, eBioscience™	Thermo Fisher Scientific	Cat# 53-0452-82; RRID: AB_469907
LYVE1 Monoclonal Antibody (ALY7), Alexa Fluor 488, eBioscience™	Thermo Fisher Scientific	Cat# 53-0443-82; RRID: AB_1633415
FITC Anti-Mouse CD11c (N418) antibody	Tonbo Biosciences	Cat# 35-0114; RRID: AB_2621677
FITC Anti-Mouse CD4 (RM4-5) Antibody	Tonbo Biosciences	Cat# 35-0042; RRID: AB_2621666
PE Anti-Mouse MHC Class II (I-A/I-E) (M5/114.15.2) antibody	Tonbo Biosciences	Cat# 50-5321; RRID: AB_2621796
Peripherin antibody	abcam	Cat # ab53051; RRID: AB_881973
APC anti-mouse CD45.1	BioLegend	Cat # 110714; RRID: AB_313503
FITC anti-mouse CD45.2	BioLegend	Cat # 109806; RRID: AB_313443
Anti-RAMP1 antibody	abcam	Cat # ab203282; RRID: AB_2924360
PE Mouse Anti-Armenian and Syrian Hamster IgG Cocktail	BD Biosciences	Cat# 554056; RRID: AB_2278421
Alexa Flour® 488 IgG1, κ Isotype Ctrl Antibody	BioLegend	Cat# 400417; RRID: AB_389319
Alexa Flour® 647 Rat IgG1, κ Isotype Ctrl Antibody	BioLegend	Cat# 400418; RRID: AB_389341
Alexa Fluor® 488 Rat IgG2a, κ Isotype Ctrl Antibody	BioLegend	Cat# 400525; RRID: AB_2864283
APC anti-mouse IgG2b Antibody	BioLegend	Cat# 406712; RRID: AB_2750278
APC Mouse IgG2a, κ Isotype Ctrl Antibody	BioLegend	Cat# 400220; RRID: AB_326468
Brilliant Violet 421™ Rat IgG2a, κ Isotype Ctrl	BioLegend	Cat# 400535; RRID: AB_10933427
FITC Armenian Hamster IgG Isotype Ctrl Antibody	BioLegend	Cat# 400905; RRID: AB_2923258
FITC Rat IgG2a, κ Isotype Ctrl Antibody	BioLegend	Cat # 400506; RRID: AB_2736919
PE anti-rat IgG2b antibody	BioLegend	Cat# 408213; RRID: AB_2728432
PE Rat IgG2a,κ Isotype Ctrl Antibody	BioLegend	Cat# 400508; RRID: AB_326530

(*Continued on next page*)

Continued

REAGENT or RESOURCE	SOURCE	IDENTIFIER
Rabbit (DA1E) mAb IgG XP® Isotype Control (Alexa® 488)	Cell Signaling Technology	Cat# 4340; RRID: AB_561545
Donkey anti-Rabbit IgG (H+L) Highly Cross-Adsorbed Secondary Antibody, Alexa Fluor™ 555	Thermo Fisher Scientific	Cat# A-31572; RRID: AB_162543
Anti-CD4 antibody [EPR6855]	abcam	Cat# ab133616; RRID: AB_2750883
Purified anti-human CD45RO Antibody	BioLegend	Cat# 304202; RRID: AB_314418
Anti-CGRP antibody [4901]	abcam	Cat# ab81887; RRID: AB_1658411
Human IL-33 Affinity Purified Polyclonal Ab antibody	R&D Systems	Cat# AF3625; RRID: AB_1151900
0.5ml NCL-L-CD19-163	Leica Biosystems	Cat# CD19-163-L-CE-H; RRID: AB_2924363
Rabbit IgG, polyclonal - Isotype Control	abcam	Cat# ab37415; RRID: AB_2631996
Mouse IgG - Isotype Control	abcam	Cat# ab37355; RRID: AB_2665484
Chemicals, Peptides, and Recombinant Proteins		
Mite, House Dust (*Dermatophagoides pteronyssinus*)	Greer Laboratories Inc.	Cat# B84
2-Hydroxypropyl-β-cylcodextrin	FUJIFILM	Cat# 324-84233
Purified Rat Anti-Mouse CD16/CD32 (Mouse BD Fc Block™)	BD Biosciences	Cat# 553141; RRID: AB_394656
eBioscience™ Fixable Viability Dye eFluor™ 780	Thermo Fisher Scientific	Cat# 65-0865-14
Recombinant Murine IL-2 Protein	homemade	N/A
Recombinant Murine IL-4 Protein	PEPROTECH	Cat# 214-14
Anti-IFN-γ monoclonal antibody	homemade	N/A
Recombinant Mouse IL-33 Protein	R&D	Cat# 3626-ML
Phorbol 12-myristate 13-acetate	Sigma-Aldrich	Cat# P1585
Ionomycin	Sigma-Aldrich	Cat# I0634
Monensin	Sigma-Aldrich	Cat# M5273
DMEM (Dulbecco's Modified Eagle Medium	Gibco	Cat# 11965-092
Albumin from chicken egg white	Sigma-Aldrich	Cat# A5503
Cholera Toxin Solution 100μg	FUJIFILM	Cat# 030-20621
TRIzol	Thermo Fisher Scientific	Cat# 15596026
Chloroquine diphosphate salt	Sigma-Aldrich	Cat# C6628
α-CGRP (mouse, rat)	Bachem AG	Cat# H-2265; RRID: AB_2924366
BMS-927711 (10mg)	Funakoshi	Cat# CS-1027
Diphenhydramine hydrochloride	Sigma Aldrich	Cat # 3630
CD124	BD Biosciences	Cat# 551853; RRID: AB_394274
NucBlue™ Fixed Cell ReadyProbes™ Reagent (DAPI)	Thermo Fisher Scientific	Cat# R37606
Target Retrieval Solution, High pH	DAKO	Cat# K8004
MAX-PO®	Nichirei Bioscience	Cat# 424144
Biotinylated Anti-mouse IgG	VECTOR	Cat# BA2000; RRID: AB_2313581
Biotinylated anti-goat IgG	VECTOR	Cat# BA5000; RRID: AB_2336126
VECTASTAIN Elite ABC Reagent	VECTOR	Cat# PK6100
TSA Cyanine3 System	PerkinElmer	Cat# SAT704A001EA
TSA Fluorescein System	PerkinElmer	Cat# SAT701001KT
Antigen activation solution, pH9	Nichirei Bioscience	Cat# 415201
BrainBits NbActiv1 neuron culture medium	Thermo Fisher Scientific	Cat# NC1588415
Brain Bits papain	Thermo Fisher Scientific	Cat# NC0319872
Collagenase from Clostridium histolyticum	Sigma-Aldrich	Cat# C5138
Hyaluronidase from sheep testes	Sigma-Aldrich	Cat# H6254
Deoxyribonuclease I from bovine pancreas	Sigma-Aldrich	Cat# DN25
Critical Commercial Assays		
Multi Tissue Dissociation kit1	Miltenyi Biotec	Cat# 130-110-201
MojoSort™ Mouse CD4 T Cell Isolation Kit	BioLegend	Cat# 480033
CD4+CD62L+ T Cell Isolation Kit II mouse	Miltenyi Biotec	Cat# 130-093-227

(*Continued on next page*)

Continued

REAGENT or RESOURCE	SOURCE	IDENTIFIER
Anti-FITC MicroBeads	Miltenyi Biotec	Cat# 130-048-701; RRID: AB_244371
TaqMan® Fast Advanced Master Mix	Thermo Fisher Scientific	Cat# 4444557
Chromium Single Cell 3' Reagent Kits v3	10x genomics	Cat# PN-1000075
SuperScript™ II Reverse Transcriptase	Thermo Fisher Scientific	Cat# 18064014
ACK Lysing Buffer	Thermo Fisher Scientific	Cat# A1049201
Alexa Fluor 647 Tyramide SuperBoost Kit, goat anti-rabbit IgG	Thermo Fisher Scientific	Cat# B40926; RRID: AB_2924369
Deposited Data		
Raw and Processed RNA-seq data	Morimoto et al. (2018)	GEO: GSE114921
Raw and Processed single cell RNA-seq data	This paper	GEO: GSE203217
Experimental Models: Organisms/Strains		
BALB/c mice	CLEA Japan	N/A
Foxn1^{nu} mice	CLEA Japan	N/A
Anti-OVA-specific TCR-αβ (DO11.10) transgenic (Tg) mice	The Jackson Laboratory	Stock No: 003303
Il33$^{-/-}$ mice	Oboki et al. (2010)	N/A
Il1rl1$^{-/-}$mice	Dr. Andrew N.J. McKenzie	N/A
ΔdblGATA mice	The Jackson Laboratory	Stock No: 033551
Ramp1$^{-/-}$ mice	The Jackson Laboratory	Stock No: 031560
Thy1.1 mice	The Jackson Laboratory	Stock No: 000406
CD4-Cre transgenic (Tg) mice	Taconic Farms	Stock No: 4196
Calca$^{fl/fl}$ mice	This paper	N/A
Oligonucleotides		
See Table S3 for qPCR	N/A	N/A
Software and Algorithms		
Flowjo v10.6.1	FlowJo LLC	https://www.flowjo.com/; RRID: SCR_008520
Prism v8.4.2	GraphPad	http://www.graphpad.com/; RRID: SCR_002798
Bowtie2 v2.0.0	Langmead and Salzberg (2012)	http://bowtie-bio.sourceforge.net/bowtie2
TopHat v1.3.2	Trapnell et al. (2009)	http://ccb.jhu.edu/software/tophat/index.shtml; RRID:SCR_013035
Cufflinks v2.0.2	Mortazavi et al. (2008)	http://cole-trapnell-lab.github.io/cufflinks/cuffmerge/; RRID:SCR_014597
illumina's bcl2fastq v2.19	Illumina	https://support.illumina.com/sequencing/sequencing_software/bcl2fastq-conversion-software.html; RRID:SCR_015058
Samtools v1.3	Li and Durbin (2009)	http://htslib.org/; RRID:SCR_002105
Bamtools v2.5.1	Derek Barnett	https://github.com/pezmaster31/bamtools/wiki; RRID:SCR_015987
R v3.6.3	R Development Core Team (2022)	https://cran.r-project.org; RRID: SCR_001905
Seurat v3.0	Stuart et al. (2019)	http://seurat.r-forge.r-project.org/; RRID:SCR_007322
Cell Ranger v4.0	10x genomics	https://support.10xgenomics.com/single-cell-gene-expression/software/pipelines/latest/what-is-cell-ranger; RRID: SCR_017344
ImageJ v1.8.0	NIH Image	https://imagej.net/; RRID:SCR_003070
Adobe Photoshop 2020 or Adobe photoshop CC	Adobe Systems Inc.	https://www.adobe.com/products/photoshop.html
Adobe Illustrator 2020	Adobe Systems Inc.	https://www.adobe.com/products/illustrator.html

(*Continued on next page*)

Continued

REAGENT or RESOURCE	SOURCE	IDENTIFIER
Other		
Multi-beads shocker® MB1001(S)	Yasui Kikai	Cat# N/A
gentleMACS™ Octo dissociator with Heaters	Miltenyi Biotec	Cat# 130-096-427
gentleMACS™ C Tubes	Miltenyi Biotec	Cat# 130-093-237
autoMACS® Pro Separator	Miltenyi Biotec	Cat# 130-092-545
BD FACSCanto™ II	BD Biosciences	Cat# N/A
BD FACSAria III Cell Sorter	BD Biosciences	Cat# N/A
Illumina NovaSeq 6000 Sequencing System	illumina	Cat# N/A; RRID: SCR_016387
BZ X-710 fluorescent microscope	Keyence	RRID: SCR_017202
Zeiss LSM 710 Confocal Inverted Microscope	Carl Zeiss	RRID: SCR_018063
Nikon A1 Confocal Laser Microscope	Nikon	RRID: SCR_020317

RESOURCE AVAILABILITY

Lead contact

Further information and requests for resources and reagents should be directed to and will be fulfilled by the Lead Contact, Toshinori Nakayama (tnakayama@faculty.chiba-u.jp).

Materials availability

Materials used in this study are available upon requests.

Data and code availability

- Raw and analyzed data reported in this paper have been deposited at GEO and are available as of the date of publication. Accession numbers are listed in the key resources table.
- This paper does not report original code.
- Any additional information required to reanalyze the data reported in this paper is available from the lead contact upon request.

EXPERIMENTAL MODEL AND SUBJECT DETAILS

Mice

The animals used in this study were backcrossed to BALB/c mice or C57BL/6 more than ten times. Anti-OVA-specific TCR-αβ (DO11.10) transgenic (Tg) mice were provided by Dr. D. Loh (Washington University School of Medicine, St. Louis). Il33$^{-/-}$ mice were generated as previously described (Oboki et al., 2010). Il1rl1$^{-/-}$ mice were kindly provided by Dr. Andrew N.J. McKenzie (Medical Research Council, Cambridge). *CD4*-Cre transgenic (Tg) mice, Δdbl-GATA mice, Thy1.1 mice, and Ramp1$^{-/-}$ mice were purchased from Taconic Farms and Jackson Laboratories, respectively. *Calca*$^{fl/fl}$ mice were generated by Drs. Satoru Takahashi and Seiya Mizuno (Tsukuba University, Ibaraki, Japan). BALB/c and *Foxn1*^{nu} mice were purchased from CLEA Japan (Tokyo, Japan). All mice were used at 6-8 weeks of age and were maintained under specific-pathogen-free conditions. Littermates of the same sex were randomly assigned to experimental groups. Both male and female mice were used in the experiments. The research proposals were reviewed and approved by the ethics committee for animals at Chiba University (registration number: A1-254, A2-121, A2-123, 3-426, 4-91).

Human samples

All participants with VKC and AKC clinically diagnosed according to the Japanese Guideline for Allergic Conjunctival Diseases received treatment at the Department of Ophthalmology in Juntendo University Hospital, or Juntendo Urayasu Hospital, Japan. Healthy controls did not have any diseases, including allergic diseases, that could affect their immune system. The participants in this study were male and female patients of 13 to 68 years of age. Detail information of the participants are described in Table S2. Samples of healthy controls and patients with VKC and AKC were collected from conjunctiva during therapeutic surgery. Total of 5 mm square specimens were obtained and classified at the Department of Ophthalmology in Juntendo University Hospital, or Juntendo Urayasu Hospital. These de-identified samples were analyzed at Chiba University. The research proposals were reviewed by the ethics committees of Juntendo University and Chiba University (registration numbers: 2019244 and 1086). Informed consent was obtained from all participants.

METHOD DETAILS

House dust mite-induced experimental allergic conjunctivitis

In advance of the experiments, *Dermatophagoides pteronyssinus* extract (Greer Laboratories Inc.) was processed into fine particles with multi-beads shocker (Yasui Kikai) five times at 3,000 rpm for 1 minute. This mite extract was administered to mice subcutaneously followed by ocular instillation: 500 μg of HDM with 20% hydroxypropyl-β-cyclodextrin (HP-β-CD) (FUJIFILM) was subcutaneously injected on days 0 and 7. On days 14 and 15, 500 μg of HDM with 20% HP-β-CD was instilled into the eyes, and then 100 μg of HDM was instilled into the eyes 5 times per week for 3 weeks. After a two-week rest period, 100 μg of HDM was given once on day 46. On days 32 and 46, scratching assays were performed as described below, then various assays were executed on days 33 and 47. In a model using BMS-927711 (Funakoshi), BMS-927711 was dissolved in DMSO and diluted in corn oil; a volume of 0.3 mg/mouse was administered intraperitoneally twice a week for 5 weeks. Based on the results of a set of preliminary experiments, we chose the protocol that used adjuvants throughout the course of the model preparation to investigate severe itch accompanied by nerve elongation. In some experiments, anti-IL-4Rα antibody (BD Biosciences) was diluted in phosphate-buffered saline; a volume of 36 μg/mouse was administered intraperitoneally twice a week from day 0 to day 45.

Histology and immunofluorescence

Pathological changes were evaluated by Haematoxylin-Eosin (H-E) staining, Giemsa staining, and immunofluorescence, as previously described (Hirahara et al., 2008; Shinoda et al., 2016). Cryostat sections (thickness, 10 μm) of mouse eye were stained and mounted with fluorescent mounting medium (DakoCytomation). Monoclonal antibodies against CD4 (RM4-5), CD45 (30-F11), anti-β-III tubulin (Tuj1), (BioLegend); anti-CD3e (145-2C11), anti-B220 (RA3-6B2), anti-CD31(390) and anti-Lyve-1 (ALY7) (Thermo Fisher Scientific); anti-OVA-TCR (KJ1.26), anti-CD21/CD35 (7G6) and anti-Ly6G (1A8) (BD Biosciences); anti-MHC class II (M5/114.15.2) and anti-CD11c (N418) (Tonbo Biosciences); were used for staining. Rabbit polyclonal antibody against Peripherin and RAMP1 (abcam) was used as the primary antibody. For the staining of Peripherin, donkey anti-rabbit IgG Alexa fluor 555 (Thermo Fisher Scientific) was used as the secondary antibody. For the staining of RAMP1, the primary antibody was detected by Alexa fluor 647 Tyramide SuperBoost Kit Goat anti-rabbit IgG (Thermo Fisher Scientific). DAPI (Thermo Fisher Scientific) was used at the end of the procedure, in accordance with the manufacturer's protocol. A fluorescence microscope (BZ-X 710, KEYENCE), confocal microscope (LSM710, Carl Zeiss), and A1 Inverted Confocal Microscope (Nikon) were used, and the images were analyzed by the ImageJ software program (National Institutes of Health).

Preparation of single-cell suspensions from tissues

Single-cell suspensions were prepared from conjunctivae of mice. After euthanasia, mice were perfused with 10 ml of cold saline solution through the left and right ventricle respectively. Conjunctivae were dissociated in a gentleMACS C-tube (Miltenyi Biotec) with digestion buffer composed of DMEM (Gibco) and Multi Tissue Dissociation Kit 1 using a gentleMACS Octo dissociator (Miltenyi Biotec). After running the program "37°C_multi_H", cell surface staining was performed for 30 minutes in a 1.5-mL microtube (eppendolf), with 15 minutes of Fc blocking (BD Biosciences) beforehand. Cell suspensions were passed through a 70-μm nylon mesh sheet.

Preparation of single-cell suspensions from trigeminal ganglia (TGs)

Freshly obtained TGs, as previously described (Katzenell et al., 2017; Zeisel et al., 2018), were immediately minced and incubated in BrainBits NbActiv1 neuron culture medium (Thermo Fisher Scientific) containing 2 mg/ml Brain Bits papain (Thermo Fisher Scientific). Homogenized products were pipetted, and spontaneous sedimentation was awaited, at which point the cells in the supernatant were collected.

Preparation of single-cell suspensions from giant papillae and peripheral blood mononuclear cells (PBMCs)

Freshly obtained giant papillae were immediately minced and incubated in RPMI 1640 medium containing 1 mg/ml collagenase, 0.5 mg/ml hyaluronidase, and 0.2 mg/ml DNase I (Sigma-Aldrich). After incubation, giant papillae were purified by the Ficoll-Hypaque technique. A volume of 1 mL of PBS was added for every 100 mg of tissue and supplemented with aprotinin and leupeptin (Roche). PBMCs were obtained similarly.

Flow cytometry and antibodies

For cell staining, cells were stained for 30 min at 4 °C with monoclonal antibodies specific for Siglec-F (E50-2440) was purchased from BD Biosciences; those for CD4 (RM4-5), Gr-1 (RB-8C5), CD45 (30-F1) and ST2 (DIH9) and isotype control were purchased from BioLegend. All cells were incubated with anti-CD16/CD32 (2.4G2; BD Biosciences) to block Fc receptors before staining with the target antibodies. 0.1% Fixable Viability Dye eFluor™ 780 (Thermo Fisher Scientific) was used to exclude dead cells. Samples were analyzed on a BD FACSCanto II flow cytometer (BD Biosciences), and flow cytometric data were analyzed with the FlowJo software program (FlowJo LLC).

Behavioral assay of scratching

Scratching bouts was recorded for 30 min after antigen re-administration or pruritogen administration on day 32 or 46 in our HDM model and on day 22 or 36 in our OVA model. Indeed, ocular instillation was performed, then mice were immediately replaced in their

clear acrylic cage and filmed for 30 minutes on the abovementioned day. The number of scratching bouts using the forepaw or the hindpaw toward the eyes was counted during playback of the film. Grooming behavior, such as strokes of the forepaws that begin behind the ears across the eyes, vibrissae or whole face were not counted.

Measurement of the axon length in conjunctival tissue

The axon length of conjunctival tissue stained with anti-β-III tubulin was outlined and quantified using a confocal laser microscope (LSM710, Carl Zeiss) attached to an image analysis system (Illustrator and Photoshop; Adobe Systems Inc., San Jose, CA, USA).

RNA Sequencing

RNA-seq was reanalyzed using a previously reported data set (GEO: GSE114921). For the data analysis, read sequences (50 bp) were aligned to the mm10 mouse reference genome (University of California, Santa Cruz December 2011) using Bowtie 2 (version 2.0.0) and TopHat (version 1.3.2). Fragments per kilobase of exon per million mapped reads (FPKM) for each gene were calculated using Cufflinks (version 2.0.2).

Single-cell RNA sequencing (scRNA-seq)

Cells of $CD45^+CD31^-$ fractions were freshly prepared from mice conjunctival tissue. Cells of $CD45^-CD31^-EpCAM^-$ fractions were freshly prepared from mouse trigeminal nerve tissue followed by $NeuN^+$ nuclei extraction using an autoMACS Sorter (Miltenyi Biotec). Cells of $CD45^+$ and $CD4^+$ fractions were freshly prepared from the giant papillae and peripheral blood of the patient. All of these cells were and sorted using a BD FACS Aria III (10,000 cells each, cell viability >98%) were encapsulated into droplets, and libraries were prepared using Chromium Single Cell 3.1' Reagent Kits v3 according to manufacturer's protocol (10X Genomics). The generated scRNA-seq libraries were sequenced using a 128 cycle (paired-end reads) with a NovaSeq 6000 (Illumina).

OVA-induced experimental allergic conjunctivitis

For the adoptive transfer experiments, OVA-specific memory Th2 cells (5×10^6 cells) were transferred into BALB/c mice or $Il33^{-/-}$ mice, and then challenged with 100 μg OVA (Sigma-Aldrich) and 0.1 μg Cholera Toxin (FUJIFILM) in 5 μl of sterile saline water per eye. The solution was instilled into the eyes five times every other day from day 0 and another five times from day 14. On days 23 and 37, various assays were performed. Based on the results of a set of preliminary experiments, we chose the protocol that used adjuvants throughout the course of the model development to investigate severe itch accompanied by nerve elongation.

Retrograde labeling

Mice repeatedly exposed to HDM were anesthetized and had Alexa Fluor 488-conjugated WGA (Thermo Fisher Scientific) injected into the subconjunctiva on day 45. The TG and dorsal root ganglion (DRG) of the mice were dissected as described before and stored in OCT compound at -70 °C on day 47. Cryostat sections (thickness, 10 μm) of mouse DRG and TG were fixed in 4% PFA and stained and mounted with fluorescent mounting medium (DakoCytomation). DAPI was used at the end of the procedure. A fluorescence microscope (BZ-X 710, KEYENCE) and confocal microscope (LSM710, Carl Zeiss) were used, and the images were analyzed by the ImageJ software program (National Institutes of Health).

Bone marrow transfer experiment

$CD45.1^+$ or $CD45.2^+$ wild-type mice and $CD45.2^+$ $Ramp1^{-/-}$ mice were irradiated with 9.5 Gy. After at least 8 h, donor mice ($CD45.1^+$ wild-type or $CD45.2^+$ $Ramp1^{-/-}$ mice) were euthanized, and bone marrow was extracted from the bilateral femurs. Bone marrow cells were incubated in ACK Lysing Buffer (Thermo Fisher Scientific), and $Thy1.2^+$ cell-depleted 1.0×10^7 bone marrow cells were intravenously injected into host mice. After 6-8 weeks, cell surface staining for Flow Cytometry against $CD45.1^+$ (clone, A20; Biolegend) and $CD45.2^+$ (clone, 104; Biolegend) was performed using PBMCs derived from the host mice to confirm the replacement of bone marrow.

Generation of effector and memory Th2 cells

Effector Th2 cells were generated as previously described (Morimoto et al., 2018). In brief, splenic $CD62L^+CD44^-KJ1^+CD4^+$ T cells from DO11.10 OVA-specific TCR Tg mice were stimulated with an OVA peptide (Loh15, 1 μM) plus antigen-presenting cells (irradiated splenocytes) under Th2-cell-culture conditions (25 U/ml IL-2; homemade, 10 U/ml IL-4; PEPROTECH, and anti-IFN-γ monoclonal antibody; homemade) for 6 days *in vitro*. The effector Th2 cells (5×10^7) were transferred intravenously into BALB/c nu/nu or BALB/c recipient mice. At five weeks after cell transfer, $KJ1^+CD4^+$ T cells in the spleen were purified by an autoMACS Sorter (Miltenyi Biotec, Bergisch Gladbach, Germany) and cell sorting (BD Aria III) and were used as memory Th2 cells for adoptive transfer. In some experiments, memory Th2 cells sorted from *Foxn1*^{nu} mice were stimulated with IL-33 (R&D) at a concentration of 10 ng/ml for 72 hours.

Quantitative Real-Time PCR

Total RNA isolation, cDNA synthesis, and quantitative real-time PCR were described previously (Ichikawa et al., 2019). Primers and Roche Universal probes were purchased from Sigma and Roche, respectively. Primers and TaqMan probes were purchased from Applied Biosystems. SuperScript™ II Reverse Transcriptase (Thermo Fisher Scientific) was used for Reverse Transcription. The

gene expression was normalized to the *Hprt or Beta-actin* mRNA signals. Quantitative real-time PCR was performed using the primer sets and the probes listed in supplemental information (Table S3).

Human samples for histochemistry and immunofluorescence

Human samples were surgically excised under local anesthesia, fixed in 10% formalin and embedded in paraffin. Anti-human CD4 (abcam), anti-human CD19 (Leica), anti-human CD45RO (BioLegend) and anti-CGRP (abcam) were used as primary antibodies for the immunofluorescence analysis. Briefly, after deparaffinization, anti-human CD4 was reacted with Biotinylated Anti-mouse IgG (VECTOR), VECTASTAIN Elite ABC Reagent (VECTOR) and TSA Cyanine3 System (PerkinElmer) after antigen activation treatment using Target Retrieval Solution, High pH (DAKO) at 95°C, according to the manufacturers' protocols. MAX-PO® (Nichirei Bioscience) and TSA Fluorescein System (PerkinElmer) were used as secondary antibodies for anti-human CD19, anti-human CD45RO and anti-CGRP. Anti-IL-33 (R&D) was stained with DAB after antigen activation using antigen activation solution, pH 9 (Nichirei Bioscience) at 95°C followed by 0.3% H_2O_2 treatment.

In this study, we used a Bielschowsky silver staining kit (ScyTek Laboratories, Inc., UT) to visualize nerve fibers and neuronal cells, because the method has been widely used to study normal and pathological morphological changes in neural tissues. In addition to light microscopy, low-vacuum scanning electron microscopy was performed (TM4000Plus, Hitachi High-Technologies, Tokyo, Japan) to analyze the section after applying an osmium coating (thickness: 2.5 nm) using the Plasma-Enhanced Chemical Vapor Deposition method (Neoc-Pro/P, Meiwafosis Co., Ltd. Tokyo, Japan) (Ogata et al., 2021). The primary antibodies of CD56 (clone MRQ-42), anti-Chromogranin A (clone KL2H10), anti-S100 (Polyclonal), and Synaptophysin (clone MRQ-40) were purchased from Roche Tissue Diagnostics. The procedures used to detect the neuronal marker expression in clinical samples were all performed with a DISCOVERY ULTRA (Roche) system using these antibodies and a Ventana OptiView DAB universal Kit (Roche) according to the manufacturer's instructions. Each sample was also counterstained with Hematoxylin II (Roche) and Bluing reagents (Roche). A fluorescence microscope (KEYENCE) and a confocal microscope (Carl Zeiss) were used, and the images were analyzed using the ImageJ software program (National Institutes of Health).

QUANTIFICATION AND STATISTICAL ANALYSIS

Statistical analyses

Data were analyzed using the GraphPad Prism software program (version 8). Comparisons between two groups were performed using a two-tailed unpaired t-test, a one-way analysis of variance (ANOVA) with Tukey's multiple comparisons test, or a two-way ANOVA with Tukey's multiple comparisons test or Seidak's multiple comparisons test. P values of <0.05 were considered to indicate statistical significance.

The analysis and graphic display of RNA-seq data

A total of 10,899 genes in which the maximum FPKM value of each gene was ≥ 1.0 were included in further analyses. The 21 ligands and ligand synthases that are related to itch were reanalyzed using a previously reported dataset (GEO: GSE114921). A volcano plot was constructed using the R software program (https://www.r-project.org/).

scRNA-seq analyses

Sequence reads from all samples were processed and aggregated using Cell Ranger (https://www.10xgenomics.com/support/single-cell-gene-expression). Aggregated data were further analyzed by Seurat (Macosko et al., 2015). Specifically, we log-normalized the expression matrix, regressed the data against the total number of UMI's detected per cell, performed a PCA analysis, used PCA dimensions 1-23 to find clusters, and finally found marker genes for these clusters. We visualized the single cell gene expression as UMAP overlays, marker gene heatmaps, Dot plots and violin plots by Seurat. Scatter plots and Pearson's correlation between the two genes were constructed by Seurat. A volcano plot was constructed using the R software program.